Analysis of quantum coherence in bismuth-doped silicon: A system of strongly coupled spin qubits

M. H. Mohammady,[1,*] G. W. Morley,[1,2,†] A. Nazir,[1,3] and T. S. Monteiro[1]

[1]*Department of Physics and Astronomy, University College London, Gower Street, London WC1E 6BT, United Kingdom*
[2]*London Centre for Nanotechnology University College London, Gordon Street, London WC1H 0AH, United Kingdom*
[3]*Blackett Laboratory, Imperial College London, London SW7 2AZ, United Kingdom*

There is a growing interest in bismuth-doped silicon (Si:Bi) as an alternative to the well-studied proposals for silicon-based quantum information processing (QIP) using phosphorus-doped silicon (Si:P). We focus here on the implications of its anomalously strong hyperfine coupling. In particular, we analyze in detail the regime where recent pulsed magnetic resonance experiments have demonstrated the potential for orders of magnitude speedup in quantum gates by exploiting transitions that are electron paramagnetic resonance (EPR) forbidden at high fields. We also present calculations using a phenomenological Markovian master equation, which models the decoherence of the electron spin due to Gaussian temporal magnetic field perturbations. The model quantifies the advantages of certain "optimal working points" identified as the $df/dB = 0$ regions, where f is the transition frequency, which come in the form of frequency minima and maxima. We show that at such regions, dephasing due to the interaction of the electron spin with a fluctuating magnetic field in the z direction (usually adiabatic) is completely removed.

I. INTRODUCTION

Beginning with the seminal proposal by Kane,[1] there has been intense interest for over a decade in the use of Si:P (Ref. 2) as qubits for quantum information processing. This donor-impurity spin-system continues to demonstrate an ever-increasing list of advantages for manipulation and storage of quantum information with currently available electron paramagnetic resonance (EPR) and nuclear magnetic resonance (NMR) technology. The Si:P system has four levels due to the electron spin $S = 1/2$ coupled to a ^{31}P nuclear spin $I = 1/2$.

The key advantages are the comparatively long decoherence times, which have been measured to be of order milliseconds for the electron spin for natural Si:P. They are of order of seconds for the nuclear spin, so the nuclear spin has been identified[1] as a resource for storing the quantum information. For all but the weakest magnetic fields (i.e., $B_0 \gtrsim 200$ G),[3] the electron and nuclear spins are uncoupled so they may be addressed and manipulated independently by a combination of microwave (mw) and radio-frequency (rf) pulses, respectively. The two possible electron-spin transitions correspond to EPR spectral lines, while the nuclear spin transitions are NMR lines. Nuclear spin flips are much slower: a π pulse in the NMR case is orders of magnitude longer than for the EPR-allowed transitions.

However, over the last year or so, there has also been increasing interest in another shallow donor impurity in silicon, the bismuth atom.[4–8] The Si:Bi system is unique in several respects: it is the deepest group V donor with a binding energy of about 71 meV, it has a very large nuclear spin, $I = 9/2$, it has an exceptionally large hyperfine coupling strength, $A/2\pi = 1.4754$ GHz. ^{209}Bi is the only naturally-occurring isotope. Recent measurements of the decoherence times in natural silicon have revealed T_2 (transverse relaxation time) times of order 30% larger than for Si:P, an effect attributed to the smaller Bohr radius of Si:Bi.[5] The dominant decoherence process is the spin diffusion,[9,10] associated with the $I = 1/2$, ^{29}Si nuclei occupying just under 5% of sites in natural silicon;

the dominant ^{28}Si isotope has no nuclear spin and thus does not contribute to the dipole-coupled flip-flop process that drives the spin diffusion. A recent study of P donors in ^{28}Si, purified to such a high degree (less than 50 ppm of ^{29}Si) that spin diffusion may be neglected, revealed T_2 times potentially up to 10 s.[11] Although studies of isotopically enriched Si:Bi have yet to be undertaken, since both species share the same ^{29}Si decoherence mechanism, T_2 times of the same order may be expected. The coupling with ^{29}Si was investigated in Ref. 8. The very large nuclear spin $I = 9/2$ and associated large Hilbert space may provide a means of storing more information.[4] Efficient hyperpolarization of the system (to about 90%) was demonstrated experimentally in Ref. 6.

The present study investigates the implications of the very large hyperfine coupling, $A/2\pi = 1.4754$ GHz of Si:Bi as well as its large nuclear spin. Mixing of the Zeeman sublevels $|m_S,m_I\rangle$, achieved in the regime where the hyperfine coupling competes with the external field, which we call the "intermediate-field regime," is not unexpected and has even been investigated for Si:P for weak magnetic fields.[3] However, for Si:Bi, this regime is attained for magnetic fields $B \simeq 0.1$–0.6 T, which are moderate, but within the normal EPR range. In a previous paper,[7] we identified interesting consequences in this range of magnetic fields. Because the Rabi oscillation speed of a spin is dependent on its coupling strength to an external oscillating magnetic field, and the ratio of nuclear to electron coupling strengths is 2.488×10^{-4}, EPR pulses are orders of magnitude faster than NMR ones. We identified a set of four states of Si:Bi, which are, at high fields, entirely analogous to the four-level subspace of Si:P. At the stated magnetic field range, all four possible transitions required for two-qubit universal quantum computation may be driven by fast EPR pulses (on a nanosecond timescale), while in Si:P, two of the transitions require slow NMR pulses. A recent experimental study using an S-band (4 GHz) pulsed EPR spectrometer[12] demonstrated the possibility of this strategy in Si:Bi.

Furthermore, we identified a set of special magnetic field values: we show that here, the effect of the external field is wholly or partly canceled by a component of the hyperfine interaction. We refer to this set of field values as "cancellation resonances." We show that the cancellation resonance points are closely associated with minima and maxima of the EPR spectral frequencies, (i.e., where $df/dB = 0$). We discuss an interesting analogy with the electron spin echo envelope modulation (ESEEM) phenomenon of "exact cancellation"[13] where like for the cancellation resonances, the system Hamiltonian takes a simpler form. In exact cancellation, this leads to insensitivity to certain types of ensemble averaging. In Ref. 7, it was found that an analogous insensitivity to ensemble averaging over spin-exchange perturbations was seen at these points.

Here, we investigate decoherence near the $df/dB = 0$ points. In particular, we consider effects of Gaussian temporal magnetic-field fluctuations along the x and z directions on decoherence. We label these X noise and Z noise, respectively. These may be relevant to the behavior of isotopically enriched Si:Bi. We show that for Z noise, which is usually adiabatic, the $df/dB = 0$ points offer decoherence-free zones. In analogy with work done on superconducting qubits,[14] we call these "optimal working points." The system does not show such advantages for X noise, however, which leads to temperature-independent depolarising noise.

In Sec. II, we follow our previous study[7] by presenting a full discussion of the spectral line positions and transition strengths for coupled nuclear-electronic spin systems for $S = 1/2$ and arbitrary I. We show that systems with large A and I display a rich structure of new EPR transitions, many of which are forbidden at high fields (even as NMR transitions) and present a set of selection rules to classify four distinct types of transitions. We discuss the cancellation resonance points and explain their relation to the maxima and minima of the transition frequencies. In Sec. III, we introduce the system as a pair of coupled qubits and compare with Si:P. We propose here a scheme of universal two-qubit quantum computation in the intermediate-field regime, exploiting transitions forbidden at high field to obtain an orders of magnitude speedup relative to conventional Si:P qubits, which must combine fast EPR manipulation with much slower NMR. In Sec. IV, we introduce a model of decoherence caused by a temporal fluctuation of the external magnetic field and study the effect of the cancellation resonances on the decoherence rates this model predicts. We conclude in Sec. V.

II. THEORY OF COUPLED NUCLEAR-ELECTRONIC SPIN SPECTRA

A. The Hamiltonian

Nuclear-electronic spin systems such as Si:P and Si:Bi are described by the Hamiltonian:

$$\hat{H}_0 = \omega_0 \hat{S}_z - \omega_0 \delta \hat{I}_z + A\hat{\mathbf{S}} \cdot \hat{\mathbf{I}}, \tag{1}$$

where ω_0 represents the electron Zeeman frequency given by $Bg\beta$. Here, B is the strength of the external magnetic field along the z direction, g is the electron g factor, and β is the Bohr magneton. $\delta = \omega_I/\omega_0 = 2.488 \times 10^{-4}$ represents the ratio of

the nuclear to electronic Zeeman frequencies. A is the isotropic hyperfine interaction strength. The operators $\hat{\mathbf{S}}$ and $\hat{\mathbf{I}}$ act on the electronic and nuclear spins, respectively.

For the systems considered, the electron spin is always $S = 1/2$. As a result, the dimension of the Hilbert space is determined by the particular nuclear spin: for a given nuclear spin I, there are $2(2I + 1)$ eigenstates, which can be superpositions of spin basis states $|m_S, m_I\rangle$. However, since $[\hat{H}_0, \hat{S}_z + \hat{I}_z] = 0$, the Hamiltonian in Eq. (1) decouples to a direct sum of one and two-dimensional sub-Hamiltonians H_m^{1d} and H_m^{2d} with constant $m = m_S + m_I$. The former act on the basis states $|m_S = \pm\frac{1}{2}, m_I = \pm(I + \frac{1}{2})\rangle$, while the latter act on the basis states $|m_S = \pm\frac{1}{2}, m_I = m \mp \frac{1}{2}\rangle$ such that $|m| < I + \frac{1}{2}$. The two-dimensional sub-Hamiltonians can be expanded in the Pauli basis. In particular, the external field part of the sub-Hamiltonian operator is given by

$$\omega_0 \hat{S}_z - \omega_0 \delta \hat{I}_z = \frac{\omega_0}{2}[(1 + \delta)\sigma_z - 2m\delta\mathbb{1}]. \tag{2}$$

The z component of the hyperfine coupling,

$$A\hat{S}_z \otimes \hat{I}_z = \frac{A}{2}(m\sigma_z - \mathbb{1}/2), \tag{3}$$

is seen to have an isotropic component as well as a nonisotropic component dependent on σ_z, while the x and y components are given by

$$A(\hat{S}_x \otimes \hat{I}_x + \hat{S}_y \otimes \hat{I}_y) = \frac{A}{2}\left[I(I+1) + \frac{1}{4} - m^2\right]^{1/2}\sigma_x. \tag{4}$$

Summing the above terms gives each H_m^{2d}, whereas only Eqs. (2) and (3) contribute to H_m^{1d}:

$$H_m^{2d} = \frac{A}{2}\left(\Delta_m \sigma_z + \Omega_m \sigma_x - \epsilon_m \mathbb{1}\right),$$

$$H_{m=\pm(I+\frac{1}{2})}^{1d} = \frac{A}{2}(\pm\Delta_m - \epsilon_m),$$

$$\Delta_m = m + \tilde{\omega}_0(1 + \delta), \tag{5}$$

$$\Omega_m = \left[I(I+1) + \frac{1}{4} - m^2\right]^{1/2},$$

$$\epsilon_m = \frac{1}{2}(1 + 4\tilde{\omega}_0 m\delta).$$

$\tilde{\omega}_0 = \omega_0/A$ is the rescaled Zeeman frequency. We define a parameter $R_m^2 = \Delta_m^2 + \Omega_m^2$, where R_m represents the vector sum magnitude of spin x and z components in the Hamiltonian. We denote θ_m as the inclination of R_m to the z axis, such that $\cos\theta_m = \Delta_m/R_m$ and $\sin\theta_m = \Omega_m/R_m$. Then, H_m^{2d} can also be written as

$$H_m^{2d} = \frac{A}{2}(R_m \cos\theta_m \sigma_z + R_m \sin\theta_m \sigma_x - \epsilon_m \mathbb{1}). \tag{6}$$

The range of values that θ_m can take are given by

$$\theta_m \in \begin{cases} [0, \arctan\left(\frac{\Omega_m}{|m|}\right)] & \text{when } m > 0, \\ [0, \frac{\pi}{2}] & \text{when } m = 0, \\ [0, \frac{\pi}{2} + \arctan\left(\frac{\Omega_m}{|m|}\right)] & \text{when } m < 0, \end{cases} \tag{7}$$

where the minimal value occurs as $B \to \infty$ and the maximal value occurs at $B = 0$. Note that $\theta_m < \pi \; \forall \; B$.

Straightforward diagonalization of H_m^{2d} then gives the eigenstates at arbitrary magnetic fields:

$$|\pm,m\rangle = a_m^{\pm}\left|\pm\tfrac{1}{2}, m \mp \tfrac{1}{2}\right\rangle + b_m^{\pm}\left|\mp\tfrac{1}{2}, m \pm \tfrac{1}{2}\right\rangle, \qquad (8)$$

where

$$a_m^{\pm} = \cos\left(\frac{\theta_m}{2}\right) \quad, \quad b_m^{\pm} = \pm \sin\left(\frac{\theta_m}{2}\right), \qquad (9)$$

and with the corresponding eigenenergies

$$E_m^{\pm} = \frac{A}{2}\left[-\frac{1}{2}(1 + 4\tilde{\omega}_0 m\delta) \pm R_m\right]. \qquad (10)$$

The high-field regime corresponds to $Bg\beta \gg A$. In this regime, $\theta_m \to 0$, hence $a_m^{\pm} \to 1$ and $b_m^{\pm} \to 0$; the eigenstates in Eq. (8) tend to the unmixed $|m_S, m_I\rangle$ basis states. The intermediate-field regime corresponds to $Bg\beta \sim A$ and strong mixing $|a_m^{\pm}| \sim |b_m^{\pm}|$. H_m^{1d} has $\theta_m = 0 \, \forall \, m$, and hence gives the uncoupled eigenstates $|\pm\tfrac{1}{2}, \pm(I + \tfrac{1}{2})\rangle$ at all magnetic fields. These have the simplified eigenenergies:

$$E_{m=\pm(I+1/2)} = \pm\frac{\omega_0}{2}(1 - 2\delta I) + \frac{AI}{2}. \qquad (11)$$

It is important to stress that the σ_z, σ_x above are quite unrelated to the $\hat{S}_z, \hat{S}_x$ electronic spin operators. They are simply a method of representing the two-dimensional sub-Hamiltonians.

In Fig. 1, the exact expressions in Eqs. (10) and (11) were used to reproduce the spin spectra investigated for Si:Bi in for example, Refs. 4 and 6. These equations can be used to describe any arbitrary coupled nuclear-electronic spin system obeying Hamiltonian (1), such as other donor systems in Si including P and As. However, throughout this paper, we only present numerical solutions for Si:Bi. As discussed here, its anomalously high value of A and I endows it with unique possibilities for spin-based quantum computing.

B. Selection rules and transition strengths

The strength of EPR transitions between two spin eigenstates may be characterised by a transition matrix element of typical form $|\langle\phi_i|\hat{S}_x|\phi_f\rangle|$, where the $|\phi_{i,f}\rangle$ are a pair of initial and final eigenstates involved in the transition. At high fields, $|\phi_i\rangle \equiv |m_S m_I\rangle$ and the textbook selection rules $\Delta m_S = \pm 1, \Delta m_I = 0$ determine which transitions are EPR allowed and have nonzero transition intensity. In turn, NMR transitions have transition matrix element $\delta|\langle\phi_i|\hat{I}_x|\phi_f\rangle|$ corresponding, at high fields, to the selection rule $\Delta m_I = \pm 1, \Delta m_S = 0$ for NMR-allowed transitions. The δ denotes the much weaker coupling between the nuclear magnetic dipole and the external driving field relative to the electronic spin transitions typically observed in EPR spectroscopy. Since $\delta \sim 10^{-4}$, this means that for typical, nanosecond-duration EPR driving pulses, one may safely neglect the contribution of the much smaller $\hat{I}_x$ matrix element, when calculating spin qubit rotations.

However, in the intermediate field regimes, where $Bg\beta \sim A$, the eigenstates are strongly mixed. Then, transitions with nonzero $|\langle\phi_i|\hat{S}_x|\phi_f\rangle|$ cannot be identified by the familiar NMR
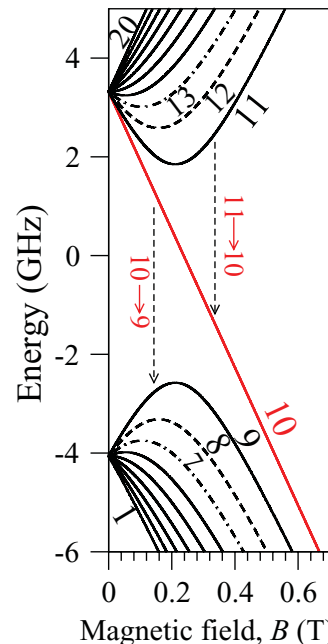

FIG. 1. (Color online) The 20 spin energy levels of Si:Bi may be labeled in order of increasing energy $|1\rangle, |2\rangle, \ldots, |20\rangle$. States $|10\rangle$ and $|20\rangle$ are not mixed. State $|10\rangle$ is of especial significance since it, rather than the ground state, is a favorable state to initialize the system in. Experimental hyperpolarization studies[6] concentrate the system in this state. Thus, in our coupled two-qubit scheme, state $|10\rangle$ corresponds to our $|0_e 0_n\rangle$ state; in the same scheme, states $|9\rangle \equiv |0_e 1_n\rangle$ and $|11\rangle \equiv |1_e 0_n\rangle$ are related to state $|10\rangle$ by a single qubit flip, while for $|12\rangle \equiv |1_e 1_n\rangle$, both qubits are flipped.

or EPR selection rules. Nevertheless, using the eigenstates in Eq. (8), we are able to identify four types of transitions that can be observed at intermediate fields: $|\pm,m\rangle \leftrightarrow |\pm,m-1\rangle$ and $|\pm,m\rangle \leftrightarrow |\mp,m-1\rangle$. For a fixed m, the first two have transition frequencies ω that differ only by $2\delta\omega_0$, and similarly for the latter two.

Transitions $|+,m\rangle \leftrightarrow |-,m-1\rangle$ are EPR allowed for all magnetic fields, and their line intensities are proportional to

$$I_{m\leftrightarrow m-1}^{+\leftrightarrow-} \propto |a_m^+|^2 |a_{m-1}^-|^2 = \cos^2\left(\frac{\theta_m}{2}\right)\cos^2\left(\frac{\theta_{m-1}}{2}\right). \quad (12)$$

In the intermediate-field regime, $|+,m\rangle \leftrightarrow |+,m-1\rangle$ transitions (of intensity $I_{m\leftrightarrow m-1}^+$) and $|-,m\rangle \leftrightarrow |-,m-1\rangle$ transitions (of intensity $I_{m\leftrightarrow m-1}^-$), which are EPR forbidden but NMR allowed, at high field, now become EPR allowed with relative intensities

$$I_{m\leftrightarrow m-1}^+ \propto |a_m^+|^2 |b_{m-1}^+|^2 = \cos^2\left(\frac{\theta_m}{2}\right)\sin^2\left(\frac{\theta_{m-1}}{2}\right) \quad (13)$$

and

$$I_{m\leftrightarrow m-1}^- \propto |a_{m-1}^-|^2 |b_m^-|^2 = \cos^2\left(\frac{\theta_{m-1}}{2}\right)\sin^2\left(\frac{\theta_m}{2}\right). \quad (14)$$

One can see from Eq. (8) that as $\omega_0 \to \infty$, the EPR intensities for these transitions goes as $I_{m\leftrightarrow m-1}^{\pm} \sim \frac{1}{\omega_0^2} \to 0$ since $|b_m^-|^2 \propto \frac{1}{\omega_0^2}$ at high fields.

However, the last transition type, namely, $|-,m\rangle \leftrightarrow |+,m-1\rangle$, is most interesting in that it is completely forbidden at high fields (it corresponds to neither an EPR-allowed nor an NMR-allowed transition at high B) but nevertheless can correspond to significant transition strengths at intermediate-field regime. These are given by

$$I_{m \leftrightarrow m-1}^{- \leftrightarrow +} \propto |b_m^-|^2 |b_{m-1}^+|^2 = \sin^2\left(\frac{\theta_m}{2}\right) \sin^2\left(\frac{\theta_{m-1}}{2}\right). \quad (15)$$

Clearly, such transitions never occur when the uncoupled eigenstates $|\pm, \pm(I + \frac{1}{2})\rangle$ are involved as these eigenstates never exhibit mixing and always obey standard EPR or NMR selection rules.

C. Cancellation resonances

As shown above, the constant m states of Eq. (8) are eigenstates of the Hamiltonian $H_m^{2d} = \frac{A}{2}(\Delta_m \sigma_z + \Omega_m \sigma_x)$ [given by Eq. (5) excluding a trivial shift], where $\Delta_m \simeq m + \tilde{\omega}_0$. For the Si:Bi spectra of Fig. 1, this encompasses nine pairs of states (i.e., all except the uncoupled states $|10\rangle$ and $|20\rangle$, which are governed by the H_m^{1d}). We use the term "cancellation resonance" as a blanket term for magnetic field regimes that simplify the system Hamiltonian. There are two types of cancelation resonance: type I, $\Delta_m = 0$, taking place when $\tilde{\omega}_0 \simeq -m$, and type II, $\Delta_m = \Omega_m$, taking place when $\tilde{\omega}_0 \simeq -m + \Omega_m$.

In the Si:Bi system with $I = 9/2$, the type I cancellation resonance corresponds to $m = 0, -1, -2, -3, -4, -5$ and a set of equally spaced magnetic field values $B = 0, 0.05, \ldots, 0.21, 0.26$ T. For $-4 \leqslant m \leqslant 0$, the term in H_m^{2d} that depends on σ_z vanishes entirely at the cancellation resonance. These are associated with Landau-Zener crossings. The point at which $m + \tilde{\omega}_0 \simeq 0$ for $m = -(I + \frac{1}{2})$ also has special interest (see below) although it is not a Landau-Zener crossing. Here, $\Omega_m = 0$ too. For Si:Bi, it corresponds to $m = -5$ and $B = 0.26$ T.

The type II cancellation resonance is particularly interesting for the $m = -3, -4$ subspaces, where at $\tilde{\omega}_0 \simeq 7$, we have $H_{m=-3,-4}^{2d} \propto (\sigma_x + \sigma_z)$ (ignoring the trivial term proportional to the identity). Although the term cancellation resonance is simply a convenient label, the type I variant is somewhat reminiscent of the ESEEM phenomenon of exact cancellation; here too, the σ_z components of the Hamiltonian vanishes, leading to insensitivity to ensemble averaging. Thus we briefly discuss the parallels below.

D. Analogy with "exact cancellation"

Exact cancellation is a widely used "trick" in ESEEM spectroscopy. A coupled nuclear-electronic system with anisotropic hyperfine coupling, which is weak compared with electron spin frequencies (on the MHz scale rather than GHz scale), has a rotating frame Hamiltonian:[13]

$$\hat{H}_0 = \Omega_s \hat{S}_z + \omega_I \hat{I}_z + A_1 \hat{S}_z \otimes \hat{I}_z + A_2 \hat{S}_z \otimes \hat{I}_x. \quad (16)$$

Here, $\Omega_s = \omega_0 - \omega$ is the detuning from the external driving field and $\omega_I = \delta \omega_0$ is the nuclear Zeeman frequency. A_1 and

A_2 are secular and pseudosecular hyperfine couplings as given in standard texts.[13] At resonance, $\Omega_s = 0$. As the hyperfine terms are weak, terms like $\hat{S}_x \otimes \hat{I}_x + \hat{S}_y \otimes \hat{I}_y$ are averaged out by the rapidly oscillating (microwave) driving. The remaining Hamiltonian $\omega_I \hat{I}_z + A_1 \hat{S}_z \otimes \hat{I}_z + A_2 \hat{S}_z \otimes \hat{I}_x$ conserves m_S. For a spin $S = 1/2$, $I = 1/2$ system like Si:P, the Hamiltonian decouples into two separate 2×2 Hamiltonians $\hat{H}_{m_S = \pm \frac{1}{2}}$. In the $m_S = +1/2$ subspace,

$$\hat{H}_{m_S = +\frac{1}{2}} = \frac{1}{2}\left(\omega_I + \frac{A_1}{2}\right)\sigma_z + \frac{A_2}{2}\sigma_x, \quad (17)$$

where the Pauli matrices are defined relative to the basis $|m_S\rangle \otimes |m_I\rangle = |+\frac{1}{2}\rangle \otimes |\pm\frac{1}{2}\rangle$, while in the $m_S = -1/2$ subspace,

$$\hat{H}_{m_S = -\frac{1}{2}} = \frac{1}{2}\left(\omega_I - \frac{A_1}{2}\right)\sigma_z - \frac{A_2}{2}\sigma_x, \quad (18)$$

where the Pauli matrices are defined relative to the basis $|m_S\rangle \otimes |m_I\rangle = |-\frac{1}{2}\rangle \otimes |\pm\frac{1}{2}\rangle$. It is easy to see from Eq. (18) that if $\omega_I = A_1/2$, only the $A_2\sigma_x/2$ term remains. This is the "exact cancellation" condition. While reminiscent of hyperfine cancellations resonances, there are key differences. In particular, since the type I cancellation resonances of Eq. (5) affect both nuclear and electron spins, at $m \simeq -\tilde{\omega}_0$, the eigenstates assume a "Bell-like" form:

$$|\Psi^\pm\rangle = \frac{1}{\sqrt{2}}\left(\left|-\frac{1}{2}\right\rangle_e \otimes \left|m + \frac{1}{2}\right\rangle_n \pm \left|+\frac{1}{2}\right\rangle_e \otimes \left|m - \frac{1}{2}\right\rangle_n\right), \quad (19)$$

where the e and n subscripts have been added for clarity, to indicate the electronic and nuclear states, respectively. In contrast, for exact cancellation, they give superpositions of nuclear spin states only:

$$|\Psi\rangle = \frac{1}{\sqrt{2}}\left|-\frac{1}{2}\right\rangle_e \otimes \left(\left|+\frac{1}{2}\right\rangle_n \pm \left|-\frac{1}{2}\right\rangle_n\right), \quad (20)$$

which still permits interesting manipulations of the nuclear spin states.[15]

Note that, while exact cancellation eliminates the full Ising term $A_1 \hat{S}_z \otimes \hat{I}_z$, the EPR cancellation resonance eliminates only the nonisotropic part. Furthermore, as discussed above, cancellation resonances also have a type II variant. The $\tilde{\omega}_0 = 7$ resonance does not cancel the hyperfine coupling at all; it equalizes the Bloch vector of the states in adjacent m subspaces producing another effect.

EPR cancellation resonances are in practice a much stronger effect than exact cancellation: decohering and perturbing effects of interest in quantum information predominantly affect the electronic spins, not the nuclear spins. Exact cancellation appears in the rotating frame Hamiltonian (which contains only terms of order MHz). It will not survive perturbations approaching the GHz energy scale. The cancellation resonances, on the other hand, arise in the full Hamiltonian, eliminate large electronic terms, and can potentially thus reduce the system's sensitivity to major sources of broadening and decoherence.

It is valuable to recall a major reason why the "exact cancellation" regime is so widely exploited in spectroscopic

studies. In systems with anisotropic coupling, the spectra depend on the relative orientation of the coupling tensor and external field. Thus for powder spectra, which necessarily average over many orientations, very broad spectral features result. At exact cancellation, the simplification of the Hamiltonian is dramatically signalled by ultra-narrow spectral lines.[13] Similarly, in Ref. 7, insensitivity to perturbation by a spin ensemble, in the form of ultranarrow spectral lines, was demonstrated in the cancellation resonance regime. This motivates further investigation of the potential of the cancellation resonance points for reducing decoherence.

E. The frequency minima and maxima

In Fig. 2, we show Si:Bi spectra in the intermediate field regime, using the expressions for frequencies and transition strengths presented above. In Fig. 2(a), we show a comparison with experimental spectra, showing good agreement with line intensities and positions. A striking feature of Fig. 2(b) is a set of spectral minima and maxima of the transition frequency of several lines. These are close, but not coincident with the cancellation resonance points (indicated by arrows and labeled $-m = 0, 1, \ldots$); for instance, while the $-m = 4$ cancellation resonance corresponds to an avoided crossing between states $|11\rangle$ and $|9\rangle$, and the $-m = 3$ point corresponds to an avoided crossing between states $|12\rangle$ and $|8\rangle$, the nearby frequency minimum involves the transitions $|12\rangle \leftrightarrow |9\rangle$ and $|11\rangle \leftrightarrow |8\rangle$. In other words, it involves two states from adjacent avoided crossings. This rich EPR structure is entirely absent in (say) conventional Si:P spin systems (with $I = 1/2$ and low A), which do not have these multiple avoided crossings, at quite high magnetic fields. It is nonetheless possible to fully analyze this structure for Si:Bi without resorting to numerics.

We can show that transitions of type $|\pm, m\rangle \leftrightarrow |\mp, m-1\rangle$ have a unique B value for which $df/dB = 0$ when

$$\cos(\theta_m) \simeq -\cos(\theta_{m-1}) \qquad (21)$$

if $-I + \frac{3}{2} \leqslant m \leqslant 0$. Such a condition can only be satisfied if $\theta_m \sim \theta_{m-1} \sim \pi/2$, meaning that both states must be near a Landau-Zener-type cancellation resonance. The value of B that satisfies this is

$$B \simeq -\frac{A}{g\beta} \frac{(m-1)\Omega_m + m\Omega_{m-1}}{\Omega_{m-1} + \Omega_m}. \qquad (22)$$

Further study of these $df/dB = 0$ points shows that they are frequency minima, and they can be observed in Fig. 2(b) near the cancellation resonance points marked "0, 1, 2, 3, 4." An equivalent way of viewing the frequency minimum condition $\cos\theta_m \simeq -\cos\theta_{m-1}$ is to write

$$\begin{aligned} \theta_m &\simeq \frac{\pi}{2} - \phi, \\ \theta_{m-1} &\simeq \frac{\pi}{2} + \phi, \end{aligned} \qquad (23)$$

so the frequency minima occur when both subspaces involved are an equal "*angular distance*" away from their cancellation resonance points.

Transitions $|\pm, m\rangle \leftrightarrow |\pm, m-1\rangle$ also have a $df/dB = 0$ point when
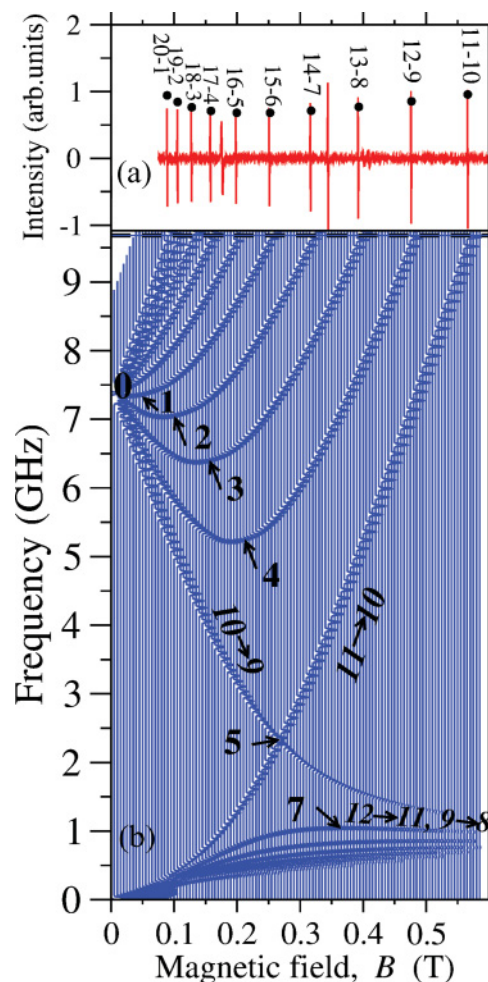
$$\cos\theta_m \simeq \cos\theta_{m-1} \qquad (24)$$

FIG. 2. (Color online) (a) Comparison between theory [see Eqs. (10), (11), and (12)] (black dots) and experimental CW EPR signal (grey/red online) at 9.7 GHz. Resonances without black dots above them are not due to Si:Bi; the large sharp resonance at 0.35 T is due to silicon dangling bonds, while the remainder are due to defects in the sapphire ring used as a dielectric microwave resonator. The variation in relative intensities is mainly due to the mixing of states as in Eq. (8). The variability is not too high but the calculated intensities are consistent with experiment and there is excellent agreement for the line positions. (b) Calculated EPR spectra (convolved with a 0.42 mT measured linewidth); they are seen to line up with the experimental spectra at $f = \omega/2\pi = 9.7$ GHz). The type I cancellation resonances are indicated by integers $-m = 0, 1, 2, 3, 4, 5$. The first four of these are associated with $df/dB = 0$ points. The type II cancelation resonance at $\tilde{\omega}_0 \simeq 7$ also coincides with a $df/dB = 0$ point, and corresponds to that shown in the $\lesssim 2$ GHz electron nuclear double resonance (ENDOR) spectra of Ref. 5. Figure reproduced with permission from Ref. 7.

if $-I + \frac{3}{2} \leqslant m \leqslant 0$. These $df/dB = 0$ points are frequency maxima and are given at fields

$$B \simeq \frac{A}{g\beta} \frac{(m-1)\Omega_m - m\Omega_{m-1}}{\Omega_{m-1} - \Omega_m}. \qquad (25)$$

Because $0 \leqslant \theta_m < \pi$, the frequency maximum condition Eq. (24) implies that $\theta_m \simeq \theta_{m-1}$. In the case of Si:Bi, only the maximum for the transitions $|\pm, -3\rangle \leftrightarrow |\pm, -4\rangle$ occurring
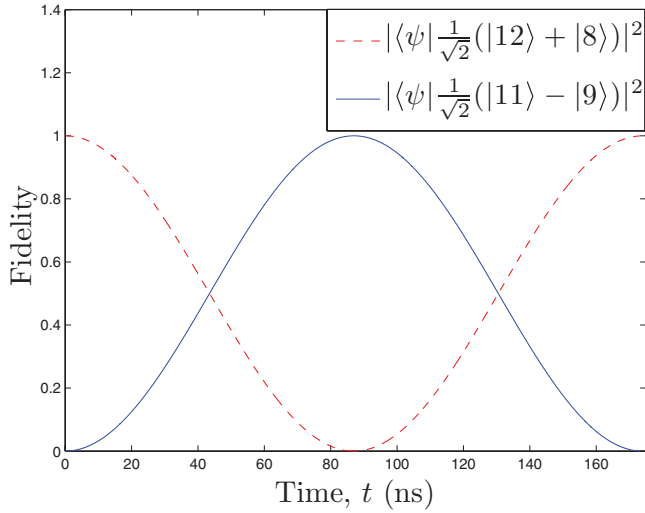
FIG. 3. (Color online) Shows that near the $\tilde{\omega}_0 = 7$ frequency maximum, the transition rates $|12\rangle \leftrightarrow |11\rangle$ and $|8\rangle \leftrightarrow |9\rangle$ equalize, and we may transfer the coherences between the former to the latter with a relative phase shift of π. We use $\omega_1/2\pi = 200$ MHz.

at $\tilde{\omega}_0 \simeq 7$ and $B \simeq 0.37$ T can be observed by EPR [this is shown in the region of Fig. 2(b) labeled "7"]. The other maxima occur at fields $B > 0.5$ T for which the EPR line intensities become vanishingly small. The $\tilde{\omega}_0 \simeq 7$ frequency maximum is especially interesting because at this value both the $m = -3, -4$ subspaces are at their type II cancellation resonance. Here, $\theta_{-3} \simeq \theta_{-4} \simeq \pi/4$, which implies that $H_{-3}^{2d} \propto H_{-4}^{2d} \propto (\sigma_x + \sigma_z)$. Such a symmetrization of the Hamiltonian offers possibilities for more complex manipulations. It has been suggested[4,5] that the larger state space of Si:Bi may be used to store more information. Thus we can show that at $\tilde{\omega}_0 \simeq 7$, a single EPR ($\sim 80$ ns) pulse can map any coherences between the $m = -4$ states into the same coherences between the $m = -3$ states. The condition of Eq. (24) implies that the amplitudes $a_{-3}^\pm \simeq a_{-4}^\pm$ and $b_{-3}^\pm \simeq \pm b_{-4}^\pm$. This means that an EPR pulse will effect the rotations $|12\rangle \leftrightarrow |11\rangle$ and $|9\rangle \leftrightarrow |8\rangle$ at the same rate. For instance, if the initial two-qubit state is $|\Psi\rangle = c_{11}|12\rangle + c_9|8\rangle$, a π pulse will yield $|\Psi\rangle = c_{11}|11\rangle - c_9|9\rangle$ and thus produces a mechanism for temporarily storing the two-qubit state (within a relative π phase shift). This is illustrated in Fig. 3.

The $m = -5$ state of Si:Bi, state $|10\rangle$, is not associated with a Landau-Zener crossing at any field as the Hamiltonian leaves it uncoupled to any other basis state. Nevertheless, the fields for which $\tilde{\omega}_0 = 5(1 + \delta)$ (at $B \approx 0.26$ T for Si:Bi) represent the most drastic case of type I cancellation resonance: the Δ_{-5} term in H_{-5}^{1d} vanishes, leaving only the ϵ_{-5} term. Here, $E_{-5} \simeq -A/4$, so its energy lies almost exactly half-way between the $|\pm, -4\rangle$ state energies: states $|9\rangle$ and $|11\rangle$ of Si:Bi have energies $E_\pm \simeq E_{-5} \pm R_{-4}$. This gives the striking feature at 2.3 GHz in Fig. 2(b) where the $|10\rangle \leftrightarrow |9\rangle$ and $|11\rangle \leftrightarrow |10\rangle$ lines coincide and where an EPR pulse would simultaneously generate coherences between state $|10\rangle$ and *both* states $|11\rangle$ and $|9\rangle$. In fact, one may use two-photon second-order processes to transfer population between states $|9\rangle$ and $|11\rangle$ (recall that simultaneous spin flips are forbidden for isotropic hyperfine coupling). Figure 4 illustrates this.
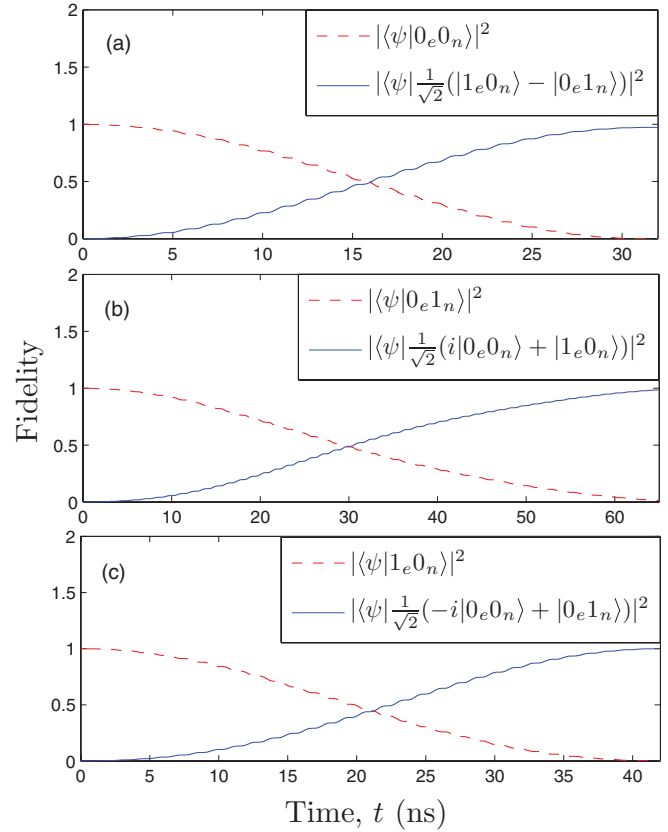

FIG. 4. (Color online) Shows that at the $\tilde{\omega}_0 = 5$ resonance, second-order two-photon transitions may be exploited since $f^{10\leftrightarrow 9} \simeq f^{11\leftrightarrow 10}$. A linear oscillating microwave field of strength $\omega_1/2\pi = 200$ MHz is used. (a) shows that driving at resonance prepares $|10\rangle \to \frac{1}{\sqrt{2}}(|11\rangle - |9\rangle)$. The process is very sensitive to detuning from resonance. (b) and (c) illustrate how slight detuning of the microwave frequency may be used to prepare other superpositions such as $|9\rangle \to \frac{1}{\sqrt{2}}(i|10\rangle + |11\rangle)$ and $|11\rangle \to \frac{1}{\sqrt{2}}(-i|10\rangle + |9\rangle)$.

III. SI:BI AS A TWO-QUBIT SYSTEM

A. Basis states

The adiabatic eigenstates of the well studied four-state $S = 1/2$, $I = 1/2$ Si:P system can be mapped onto a two-qubit computational basis, as shown in Table I.

With a 20-dimensional state space, the Si:Bi spectrum is considerably more complex. However, we can identify a natural subset of four states (states $|9\rangle, |10\rangle, |11\rangle$, and $|12\rangle$), which represents an effective coupled two-qubit analog, as shown in Table II. As hyperpolarization initializes the spins in state $|10\rangle$ (see Ref. 6) and this state has both the electron and nuclear spins fully antialigned with the magnetic field,

TABLE I. Two-qubit computational basis states of Si:P.

Adiabatic state	High-field state	Logical qubit
$|4\rangle$	$|+\frac{1}{2}, +\frac{1}{2}\rangle$	$|1_e 1_n\rangle$
$|3\rangle$	$|+\frac{1}{2}, -\frac{1}{2}\rangle$	$|1_e 0_n\rangle$
$|1\rangle$	$|-\frac{1}{2}, +\frac{1}{2}\rangle$	$|0_e 1_n\rangle$
$|2\rangle$	$|-\frac{1}{2}, -\frac{1}{2}\rangle$	$|0_e 0_n\rangle$

TABLE II. Two-qubit computational subspace of Si:Bi.

Adiabatic state	High-field state	Logical qubit
$|12\rangle$	$|+\frac{1}{2}, -3\frac{1}{2}\rangle$	$|1_e 1_n\rangle$
$|11\rangle$	$|+\frac{1}{2}, -4\frac{1}{2}\rangle$	$|1_e 0_n\rangle$
$|9\rangle$	$|-\frac{1}{2}, -3\frac{1}{2}\rangle$	$|0_e 1_n\rangle$
$|10\rangle$	$|-\frac{1}{2}, -4\frac{1}{2}\rangle$	$|0_e 0_n\rangle$

although it is not the ground state, it can be identified with the $|0_e 0_n\rangle$ state. The other states—just as in the Si:P case—are related to it by adding a single quantum of spin to one or both qubits.

For both systems, there are, in principle, four transitions that would account for all possible individual qubit operations, as listed in Table III. We show below that for Si:Bi, all qubit operations are EPR allowed for $B \sim 0.1$–0.6 T. For Si:P, this region permits EPR manipulation of only the electronic qubit flips (the first two); nuclear rotations require much slower microsecond NMR transitions. Measurement of the qubits in the computational basis has to be performed at high fields, where the adiabatic logical qubit coincides with the electron and nuclear spin states. All simultaneous nuclear and electronic qubit flips are forbidden for systems with isotropic hyperfine coupling A, including both Si:P and Si:Bi. We note that, in spin-systems with "exact cancellation" and anisotropic A, the $A\hat{I}_x \otimes \hat{S}_z$ coupling does permit simultaneous nuclear-electronic qubit flips. These were recently shown for the organic molecule malonic acid;[15] the disadvantage here is that single nuclear qubit rotations (essential for quantum computation) are not EPR allowed.

B. Universal set of quantum gates

It is known that for universal quantum computation it suffices to be able to perform arbitrary single-qubit rotations and a two-qubit gate such as the controlled-not (CNOT) gate.[16] We now show how we may exploit the strong hyperfine interaction of the Si:Bi system to achieve this using only fast EPR pulses, eliminating the need for the much slower (longer-duration) NMR pulses.

TABLE III. Conditional single-qubit rotations of angle θ about vector $\underline{v}$ in the Bloch sphere, denoted $\hat{R}_{\underline{v}}(\theta)$, and corresponding transition frequencies. Frequencies in boldface correspond to qubit operations, which are EPR allowed at $B = 0.1$–0.6 T, i.e., they require only fast (nanosecond) EPR pulses. All four EPR operations are possible for Si:Bi, whereas for Si:P, nuclear qubit operations require slow (microsecond) NMR pulses. This scheme allows for cheap, controlled qubit operations, whereas single-qubit operations would require twice the number of pulses.

Controlled operation	Si:P transitions	Si:Bi transitions
$\hat{R}_{\underline{v}}(\theta)_e \otimes |0\rangle\langle 0|_n$	$\omega^{\mathbf{3}\leftrightarrow\mathbf{2}}$	$\omega^{\mathbf{11}\leftrightarrow\mathbf{10}}$
$\hat{R}_{\underline{v}}(\theta)_e \otimes |1\rangle\langle 1|_n$	$\omega^{\mathbf{4}\leftrightarrow\mathbf{1}}$	$\omega^{\mathbf{12}\leftrightarrow\mathbf{9}}$
$|0\rangle\langle 0|_e \otimes \hat{R}_{\underline{v}}(\theta)_n$	$\omega^{2\leftrightarrow1}$	$\omega^{\mathbf{10}\leftrightarrow\mathbf{9}}$
$|1\rangle\langle 1|_e \otimes \hat{R}_{\underline{v}}(\theta)_n$	$\omega^{4\leftrightarrow3}$	$\omega^{\mathbf{12}\leftrightarrow\mathbf{11}}$

Control of the electron spins is facilitated by the Hamiltonian $\hat{H} = \hat{H}_0 + V_{x/y}(t)$ where $V_{x/y}(t) = \omega_1 \cos(\omega t)\hat{S}_{x/y}$ represents the external magnetic field oscillating along the x or y axis. This may be written as

$$V_{x/y}(t) = \frac{\omega_1}{2}[\cos(\omega t)\hat{S}_{x/y} + \sin(\omega t)\hat{S}_{y/x}]$$
$$+ \frac{\omega_1}{2}[\cos(\omega t)\hat{S}_{x/y} - \sin(\omega t)\hat{S}_{y/x}]. \quad (26)$$

We label the first component the right-handed (RH) and the second term the left-handed (LH) rotating fields. In the rotating frame between two eigenstates $|e\rangle$ and $|g\rangle$, which satisfy the selection rule $|\langle e|\hat{S}_{x/y}|g\rangle| = |\eta| > 0$, the Liouville-von Neumann equation for the reduced two-level system is

$$\frac{d\tilde{\rho}(t)}{dt} = i\frac{\omega_1\eta}{4}[\tilde{\rho}(t), \hat{\sigma}_{x/y}] \quad (27)$$

if $\omega_1 \ll \omega^{e\leftrightarrow g}$, where $\omega^{e\leftrightarrow g}$ is the transition frequency between the two eigenstates. For the transitions where the increase in energy corresponds to an increase(decrease) in total z-axis magnetization, m, the resonance condition is satisfied by the RH (LH) component of the oscillating magnetic field. This feature, which is explained in more detail in Appendix A, may be exploited for qubit manipulation involving certain transitions that are near degenerate, as will be explained in the following section. The EPR pulses at our disposal allow us to perform controlled single-qubit unitaries $R_{\underline{v}}(\theta)$ where $\underline{v}$ lies in the x-y plane. Two orthogonal Paulis suffice to generate arbitrary single-qubit unitaries[17] using at most three pulses, and we may construct the controlled $\hat{\sigma}_z$ and Hadamard gates by these pulse sequences:

$$\hat{\sigma}_z = e^{i\frac{3\pi}{2}} e^{i\frac{\pi}{2}\hat{\sigma}_y} e^{i\frac{\pi}{2}\hat{\sigma}_x},$$
$$H := \frac{1}{\sqrt{2}}(\hat{\sigma}_x + \hat{\sigma}_z) = e^{i\frac{3\pi}{2}} e^{i\frac{\pi}{2}\hat{\sigma}_x} e^{i\frac{3\pi}{4}\hat{\sigma}_y} e^{i\pi\hat{\sigma}_x}. \quad (28)$$

The possible controlled operations are shown in Table III. Single-qubit gates would require us to repeat the set of controlled EPR pulses for both the controlling qubit basis states and, as such, would require twice the time.

The transition strengths given in Eqs. (12), (13), (14), and (15) are given by $|\eta|^2$. Equation (27) shows that the qubit rotation speed, given a fixed microwave field strength, is determined by the mixing factor η. As $B \to \infty$, $\eta \to 1$ for high-field EPR transitions, and $\eta \to 0$ for high-field NMR transitions as well as the high-field dipole-forbidden transition. At magnetic fields where $A \sim Bg\beta$, however, mixing occurs and η will become appreciable.

At the $m = -4$ cancellation resonance, corresponding to field values $\tilde{\omega}_0 \simeq 4$ ($B \simeq 0.21$ T), the values of $|\eta|$ for both nuclear and electronic qubit operations equalize: this is simple to verify from Eqs. (12)–(14) by setting $\theta_{-5} = 0$ and $\theta_{-4} = \pi/2$. We show numerically in Figs. 5(a)–5(b) that this means that a π pulse on the nuclear qubit in effect becomes as short as on the electronic one.

C. Selective qubit gates for near-degenerate transitions

An important advantage of using the Si:Bi at intermediate fields is the prospect of quantum computing using exclusively fast, nanosecond EPR pulses. Nevertheless, such
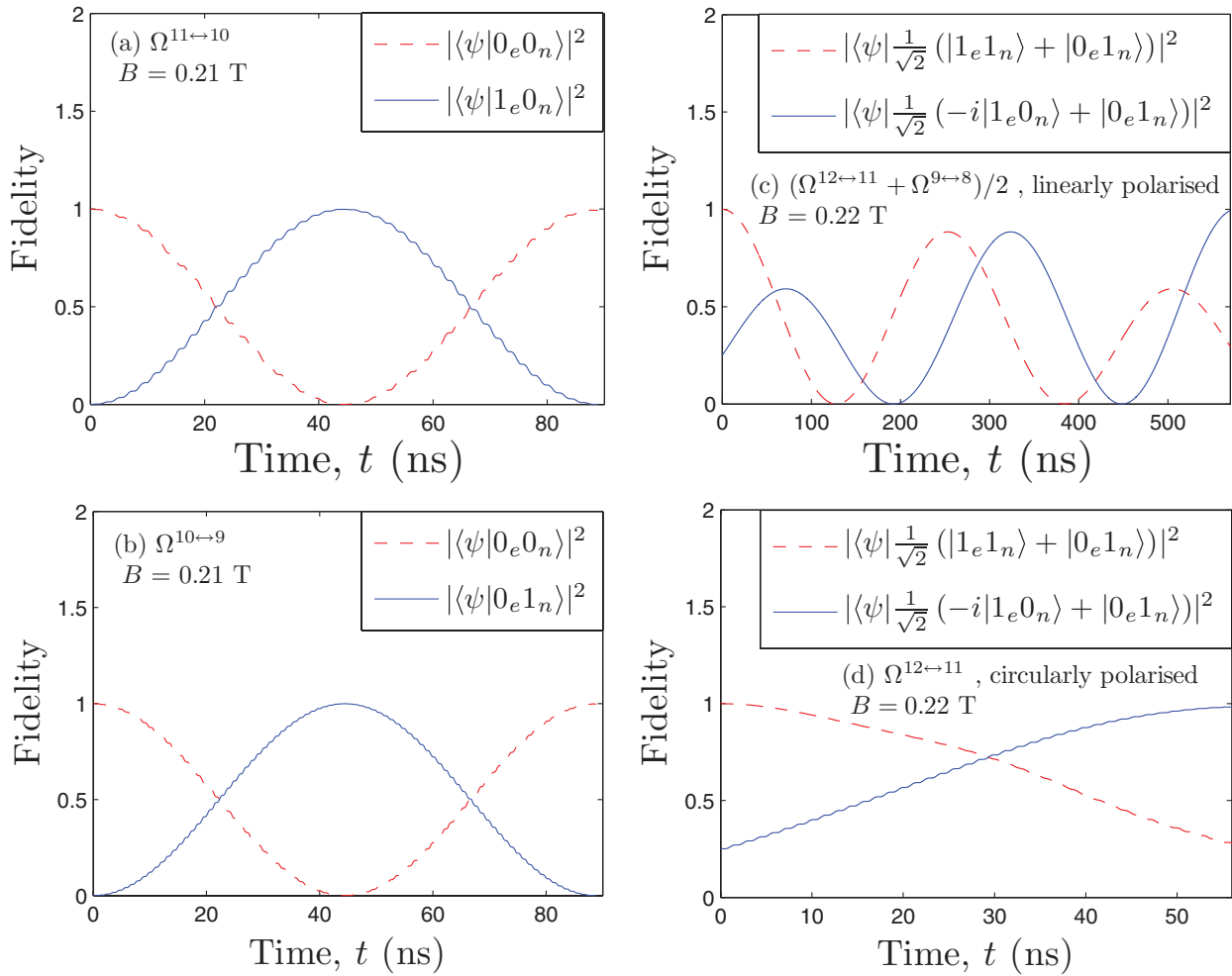
FIG. 5. (Color online) (a) and (b) show Rabi oscillations utilizing a linearly oscillating microwave field of strength $\omega_1/2\pi = 200$ MHz. At $B = 0.21$ T, the time taken for the electron qubit flip $|0_e0_n\rangle \rightarrow |1_e0_n\rangle$ is identical to that for the nuclear qubit flip $|0_e0_n\rangle \rightarrow |0_e1_n\rangle$. (c) and (d) show selective nuclear qubit flips and have microwave fields of strength $\omega_1/2\pi = 100$ MHz. This is because the energy difference between the eigenstates is smaller than in the previous two cases and ω_1 must remain perturbative. (c) Utilizes a linearly oscillating microwave field, which is nonselective for short pulses. At $B = 0.22$ T, the rotation speed ratio is $|\eta_{12\leftrightarrow 11}|/|\eta_{9\rightarrow 8}| = 5/4$. A 5π rotation of the nuclear qubit corresponds to a 4π rotation of the unwanted $|9\rangle \rightarrow |8\rangle$ transition. In (d), we use a RH circularly polarized microwave field, which selects for the desired conditional nuclear qubit rotation and is much more efficient than the linearly polarized case.

short pulses necessarily imply a larger frequency bandwidth. While this is not, in general, a problem, it may present difficulties for certain pairs of transitions that are quite close in frequency (tens of MHz rather than GHz): the EPR pulse may drive unwanted spin flips. One solution is to simply lengthen the duration of the pulse; however, one then loses much of the speedup advantage as timescales comparable to NMR are then required. We show here that it remains possible to perform selective one-qubit gates with fast EPR pulses.

For example, consider the initial state $|\psi\rangle = \frac{1}{\sqrt{2}}(|1_e1_n\rangle + |0_e1_n\rangle)$. If we wanted to perform a CNOT gate on this state, with the electron qubit as the control, we might choose to use the transition frequency $\omega^{12\leftrightarrow 11}$ as dictated by Table III. However, this frequency is only a few MHz different from that of $\omega^{9\leftrightarrow 8}$, and a short pulse of ~50 ns

would also drive the transition between states $|9\rangle$ and $|8\rangle$, and thereby effect a unwanted operation on our qubits. There are two strategies to overcome this complication: (1) by tuning the microwave frequency to be exactly between the wanted and unwanted transition frequencies and assuming a square pulse, we ensure they are both affected by the same pulse power $\omega'_1 = \omega_1 \mathrm{sinc}(T \delta\omega_0)$, where T is the pulse duration, such that the only variable affecting the two transition rates would be the mixing factor η. Near the $m = -4$ cancellation resonance at $B = 0.22$ T, we get $|\eta_{12\rightarrow 11}|/|\eta_{9\rightarrow 8}| = 5/4$. This ensures that at time $t = 10\pi/(\omega'_1|\eta_{12\rightarrow 11}|)$, we have performed the operation

$$\frac{1}{\sqrt{2}}(|1_e1_n\rangle + |0_e1_n\rangle) \rightarrow \frac{1}{\sqrt{2}}(-i|1_e0_n\rangle + |0_e1_n\rangle). \quad (29)$$

This is shown numerically in Fig. 5(c).

(2) The transition $|12\rangle \rightarrow |11\rangle$ utilizes the RH component of the microwave field, whereas the $|9\rangle \rightarrow |8\rangle$ transition uses the LH one. By generating a RH circularly polarized microwave field, we would be able to select for the desired transition, as shown in Fig. 5(d).

Obviously, scheme 2 is preferable as it requires much shorter times to carry out our quantum gates. This scheme can be used in selecting for one of the transitions $|\pm,m\rangle \leftrightarrow |\mp,m-1\rangle$, which differ in frequency by $2\delta\omega_0$, and, similarly, for transitions $|\pm,m\rangle \leftrightarrow |\pm,m-1\rangle$.

D. Scaling with controllable Heisenberg interaction

So far, we have only described how to perform two-qubit gates in a single site of Si:Bi (or any other nuclear-electronic system obeying the same Hamiltonian and with a large enough hyperfine exchange term). This is very limited, however, and we need to be able to scale the system so as to incorporate arbitrarily large numbers of qubits. With Si:Bi, the possibility does exist to further utilize the 20-dimensional Hilbert space, which would provide a maximum of four qubits. This is, however, not scalable, and we will still be limited to just four qubits as we cannot create more energy levels within the single-site Si:Bi system. The only feasible option that remains is to have spatially separated Si:Bi centers between which we can establish an interaction. The original Kane proposal[1] envisaged a Heisenberg interaction between nearest-neighbor electrons, which could be controlled via changing the electrostatic potential barrier between the donor sites, that, in turn, alters the degree of electron wave function overlap. This interaction has the effective form:

$$\hat{H}_{\text{int}} = J\hat{\mathbf{S}}^i \cdot \hat{\mathbf{S}}^{i+1}. \tag{30}$$

The same interaction could be achieved indirectly by modulating the Rydberg state of a control dopant placed in between the two qubits.[18] As shown by Ref. 19, such an interaction can be used to produce a $\sqrt{\text{SWAP}}$ gate:

$$\sqrt{\text{SWAP}} = e^{i\frac{\pi}{8}} e^{-i\frac{\hat{H}_{\text{int}}}{J}\frac{\pi}{2}}. \tag{31}$$

Using two such gates, together with single-qubit unitaries, we can establish a CZ gate between the electrons:

$$\text{CZ}^{12} = e^{i\frac{\pi}{2}} \left(e^{-i\hat{\sigma}_z^1 \frac{\pi}{4}} \otimes e^{i\hat{\sigma}_z^2 \frac{\pi}{4}}\right)\sqrt{\text{SWAP}} e^{-i\hat{\sigma}_z^1 \frac{\pi}{2}}\sqrt{\text{SWAP}}. \tag{32}$$

As stated in previous sections, we cannot perform rotations about the z axis of the Bloch sphere directly, but we can use our EPR pulses about the x and y axes to produce the required single-qubit unitaries:

$$e^{-i\hat{\sigma}_z^1 \frac{\pi}{4}} = e^{i\pi} e^{-i\hat{\sigma}_y^1 \frac{3\pi}{4}} e^{-i\hat{\sigma}_x^1 \frac{\pi}{4}} e^{-i\hat{\sigma}_y^1 \frac{\pi}{4}}. \tag{33}$$

The CZ gate can be turned into a CNOT gate by simply applying a Hadamard on the target qubit before and after the application of the CZ. Such an interaction affects the electron spin basis states, and not the adiabatic basis states to which we have designated our logical qubits. Therefore we must apply our electronic two-qubit gates in the high-field limit where mixing is suppressed and where there is a high fidelity between the adiabatic basis and spin basis. A consequence of this is that the energy difference between different eigenstates will be very large and, as is well known,[20] if $|E_i - E_{i+1}| \gg J$, the

Heisenberg interaction between the two effectively becomes an Ising interaction $J\hat{S}_z^1 \otimes \hat{S}_z^2$. To use the above scheme of producing entangling two-qubit gates between all four eigenstates in each of the two adjacent sites, we would have to establish a very strong J.

Alternatively, we can set B_i and B_{i+1} to be sufficiently different, and J small enough, such that we only get an Ising interaction between all relevant eigenstates. It is in fact easier to produce the CZ and CNOT gates with an Ising interaction, as it only requires one exchange operation and not two as in the case of the Heisenberg interaction:[21,22]

$$\text{CZ}^{12} = e^{-i\frac{\pi}{4}} \left(e^{i\hat{\sigma}_z^1 \frac{\pi}{4}} \otimes e^{i\hat{\sigma}_z^2 \frac{\pi}{4}}\right)e^{-i\hat{S}_z^1 \otimes \hat{S}_z^2 \pi}. \tag{34}$$

IV. DECOHERENCE FROM TEMPORAL MAGNETIC FIELD FLUCTUATIONS

For practical quantum information processing in silicon, the substance would need to be purified so as not to contain any ^{29}Si such that no decoherence would result due to spin-bath dynamics. Temperatures would also be maintained at low levels in order to minimize the phonon-bath-induced decoherence. Here, we wish to employ a phenomenological model of decoherence for nuclear-electronic systems, resulting only from stochastic magnetic-field fluctuations. Taking the Hamiltonian from Eq. (1) and adding to it a perturbative term involving independent temporal magnetic-field fluctuations in all three spatial dimensions (with the usual association of $1 = x, 2 = y, 3 = z$), all of which take a Gaussian distribution with mean 0 and variance α_n^2, gives in the interaction picture:

$$\tilde{H}(t) = \sum_{n=1}^3 \omega_n(t)\tilde{S}_n(t) + \omega_n(t)\delta\tilde{I}_n(t), \tag{35}$$

where $\{S_n\}$ and $\{I_n\}$ are the n-axis electron and nuclear spin operators, respectively, and $\omega_n(t)$ is the electron Zeeman frequency at time t. As before, δ represents the ratio of the nuclear to electronic Zeeman frequencies and because it is small, we may ignore the nuclear term. We then follow the standard procedure of deriving a Born-Markov master equation:[23]

$$\frac{d}{dt}\langle\rho(t)\rangle = i[\langle\rho(t)\rangle, \hat{H}_0]$$
$$+ \alpha_n^2 \sum_{n=1}^3 \sum_{\Omega} e^{-\chi_n \Omega^2} \left\{\hat{S}_n^\dagger(\Omega)\langle\rho(t)\rangle\hat{S}_n(\Omega)\right.$$
$$\left. - \frac{1}{2}[\langle\rho(t)\rangle, \hat{S}_n^\dagger(\Omega)\hat{S}_n(\Omega)]_+\right\}, \tag{36}$$

where $\hat{S}_n(\Omega)$ are the electron spin operators in the eigenbasis of $\hat{H}_0$, Ω is the energy difference between two such eigenstates, and $\chi_n = (dB_n/dt)^{-1}$ is the inverse of the rate of change of the magnetic field strength in direction n. $\langle\rho(t)\rangle$ is defined as the density operator of the coupled nuclear-electronic system, averaged over either an ensemble of such systems, or repeated experiments on a single system. Further details for the derivation of Eq. (36) can be found in Appendix B.

The rate term $e^{-\chi_n \Omega^2}$ imposes the results of the adiabatic theorem into our master equation. The quantitative condition for adiabatic evolution is often cited as[24]

$$\left| \frac{\langle \phi_i | \dot{H}(t) | \phi_j \rangle}{\Omega^{i \leftrightarrow j^2}} \right| \ll 1. \qquad (37)$$

For the model described here, this translates to

$$\left| \frac{\langle \phi_i | \hat{S}_n | \phi_j \rangle \frac{dB_n}{dt}}{\Omega^{i \leftrightarrow j^2}} \right| = |\langle \phi_i | \hat{S}_n | \phi_j \rangle| \frac{1}{\chi_n \Omega^{i \leftrightarrow j^2}} \ll 1, \quad (38)$$

which means that, in the case of $\left| \langle \phi_i | \hat{S}_n | \phi_j \rangle \right| > 0$, if the magnetic field is fluctuating sufficiently slowly, the probability of transition between eigenstates $|\phi_i\rangle$ and $|\phi_j\rangle$ becomes vanishingly small.

Since we have made the rotating wave (or secular) approximation and are only interested in the interaction picture dynamics of our system, we may drop the Hamiltonian commutator in Eq. (36), leaving only the dissipator term. For Si:Bi in the intermediate-field regime, the secular approximation can be made by setting $\alpha^2/2\pi = 9$ MHz, and we use this value whenever we provide numerical calculations. We are now equipped with the tools to address decoherence in our quantum system. We may model our gates as ideal unitaries that can prepare some superposition $|\psi\rangle = a|e\rangle + b|g\rangle$ between the adiabatic basis states $|e\rangle$ and $|g\rangle$, which is then decohered according to our noise model. The dephasing and depolarising rates are determined by applying our master equation and measuring the rate that the observables

$$\sqrt{\mathrm{tr}[\sigma_x \tilde{\rho}(t)]^2 + \mathrm{tr}[\sigma_y \tilde{\rho}(t)]^2} \qquad (39)$$

and

$$\mathrm{tr}[\sigma_z \tilde{\rho}(t)] \qquad (40)$$

decay respectively. In the cases that these decay as $e^{-\Gamma t}$, where Γ is the decay rate, we may characterize the dephasing and depolarising times by T_2 and T_1, respectively, which are the inverse of the decay rates. Such times are measured in EPR experiments.[25,26] The Pauli matrices denoted here are in the eigenbasis of the reduced two-level system in question. We will study two types of noise: Z and X noises, so named due to Gaussian magnetic-field fluctuations in the z and x axes, respectively. Throughout this section, when an adiabatic state is indicated with m, it is implied that $|m| < (I + \frac{1}{2})$, and states where $m = \pm(I + \frac{1}{2})$ are explicitly designated.

A. Z noise

Given Z noise, we may consider our system as a decoupled four-level system with sub-Hamiltonian

$$H_{\mathrm{sub}} = H_m^{2d} \oplus H_{m-1}^{2d}. \qquad (41)$$

This is possible as there will be no transfer of population to other components of the Hilbert space. We may write $\hat{S}_z$ in the adiabatic basis $\{|+,m\rangle, |-,m\rangle, |+,m-1\rangle, |-,m-1\rangle\}$:

$$\begin{pmatrix} \cos(\theta_m) & -\sin(\theta_m) & 0 & 0 \\ -\sin(\theta_m) & -\cos(\theta_m) & 0 & 0 \\ 0 & 0 & \cos(\theta_{m-1}) & -\sin(\theta_{m-1}) \\ 0 & 0 & -\sin(\theta_{m-1}) & -\cos(\theta_{m-1}) \end{pmatrix}. \qquad (42)$$

Substituting this into Eq. (36) and considering it in the interaction picture gives

$$\frac{d}{dt} \langle \tilde{\rho}(t) \rangle = \sum_{n=m-1}^{m} \frac{\alpha^2}{4} \cos^2(\theta_n) \left[\hat{\sigma}_z^n \langle \tilde{\rho}(t) \rangle \hat{\sigma}_z^n - \langle \tilde{\rho}(t) \rangle \right] + \frac{\alpha^2}{4} e^{-\chi \Omega^2}$$
$$\times \sin^2(\theta_n) [|+,n\rangle\langle -,n| \langle \tilde{\rho}(t) \rangle |-,n\rangle\langle +,n|$$
$$- |+,n\rangle\langle -,n||-,n\rangle\langle +,n| \langle \tilde{\rho}(t) \rangle + \mathrm{H.c.}]. \qquad (43)$$

In the high-field limit, our EPR local unitaries can only create superpositions $a|+,m\rangle + b|-,m-1\rangle$. As the noise operator takes the form $\hat{\sigma}_z^m \oplus \hat{\sigma}_z^{m-1}$ in this regime, this superposition may be considered to exist as a decoupled two-level system. We may therefore solve Eq. (43) (for the two-level subspace in question) analytically:

$$e^{\mathcal{L}t} \tilde{\rho}(t_0) = \frac{1}{2} \left(1 + e^{-\frac{t}{T_2}} \right) \tilde{\rho}(t_0) + \frac{1}{2} \left(1 - e^{-\frac{t}{T_2}} \right) \hat{\sigma}_z \tilde{\rho}(t_0) \hat{\sigma}_z, \quad (44)$$

where $\mathcal{L}$ is the Liouville superoperator, whose action on ρ is given by Eq. (43). This is simply the dephasing channel for a spin 1/2 particle:[17]

$$\mathcal{E}(t) \circ \rho = [1 - \lambda(t)]\rho + \lambda(t)\hat{\sigma}_z \rho \hat{\sigma}_z \qquad (45)$$

with probability $\lambda(t)$ of performing a $\hat{\sigma}_z$ operation under conjugation. Here, $\lambda(t) = (1 - e^{-t/T_2})/2$ with a T_2 time of
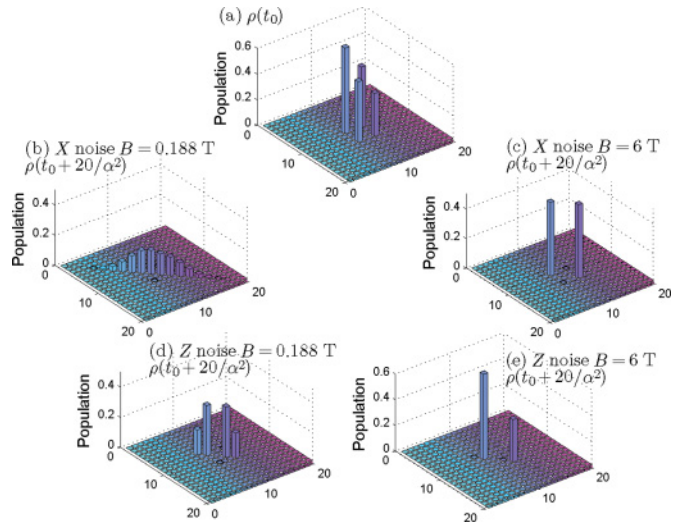

FIG. 6. (Color online) Shows the change in density operator elements of $|\psi\rangle = \frac{2}{\sqrt{3}}|9\rangle + \frac{1}{\sqrt{3}}|12\rangle$ after a period of $20/\alpha^2$, given diabatic Gaussian noise of variance α^2, at two field regimes: the frequency minimum of $B = 0.188$ T and $B = 6$ T. (a) Population of ρ in the eigenbasis of $\hat{H}_0$ at time t_0. (b) and (c) show the effect of B on X noise. (b) Near the frequency minima, X noise couples every part of the full Hilbert space, and depolarizes the full system, ultimately resulting in $\frac{1}{20}\mathbb{1}$. (c) At $B = 6$ T, X noise decouples states $|+,m\rangle, |-,m-1\rangle$ from the rest of the Hilbert space, and effects a depolarizing channel in that subspace only. (d) and (e) show the effect of B on Z noise. Z noise conserves angular momentum and hence keeps to the four-dimensional Hilbert space of $m = -3, m - 1 = -4$. (d) shows that at the frequency minimum, Z noise effects independent depolarizing channels for each m subspace. As a result, the population of states $|12\rangle$ and $|9\rangle$ equalize with those of states $|8\rangle$ and $|11\rangle$, respectively. (e) shows that at $B = 6$ T, $\langle +,m|\hat{S}_z|-,m\rangle \sim 0$ and we simply get a dephasing channel for the $|+,m\rangle, |-,m-1\rangle$ subspace.

$2/\alpha^2$. This is illustrated by Fig. 6(e), where only the off-diagonal elements of $\rho(t_0)$, as shown in Fig. 6(a), decay. At low fields, however, $\langle +,m|\hat{S}_z|-,m\rangle > 0$ and we cannot ignore the exchange term in Eq. (43). In this case, we may use the four-dimensional Bloch vector representation of our density operator:

$$\rho(t) = \frac{1}{4}\left(\sum_{i,j=0}^{3} n_{ij}(t)\hat{\sigma}_i \otimes \hat{\sigma}_j \right), \quad n_{00}(t) = 1. \quad (46)$$

It is possible to map the dynamics of the density operator to that of the Bloch vector[27] as

$$\frac{d\underline{\mathbf{n}}(\mathbf{t})}{dt} = \mathcal{L}\underline{\mathbf{n}}(\mathbf{t}). \quad (47)$$

For Si:Bi, the 16 simultaneous differential equations can be solved to obtain analytic expressions for the dephasing and depolarising rates. Alternatively, by decomposing $\underline{\mathbf{n}}(\mathbf{t})$ in the eigenbasis of $\mathcal{L}$, denoted $\underline{\mathbf{n}}_\mathbf{l}$ with generally complex eigenvalues λ_l, we may represent the dynamics of the Bloch vector as

$$\underline{\mathbf{n}}(t) = \sum_{l=0}^{15} c_l \underline{\mathbf{n}}_\mathbf{l} \mathbf{e}^{t\lambda_l}, \quad (48)$$

where c_l are determined by the initial conditions. It is the real component of the eigenvalues which leads to decay in population of the eigenstate. The infinite-time state is therefore a superposition of eigenstates $\underline{\mathbf{n}}_\mathbf{l}$ such that $\mathrm{Re}(\lambda_l) = 0$.

1. Adiabatic Z noise

Here, we may set $\chi \to \infty \Rightarrow e^{-\chi\Omega^2} = 0$ for $\Omega^2 > 0$. There will be no depolarization in this case, and we may only have pure dephasing. For superpositions of type $a|\pm,m\rangle + b|\mp,m-1\rangle$, the dephasing rate, parameterized as the decay of the off-diagonal elements of the subspace in question, is given by

$$\frac{1}{T_2} = \frac{\alpha^2}{8}[\cos(\theta_m) + \cos(\theta_{m-1})]^2. \quad (49)$$

When $\cos(\theta_m) = -\cos(\theta_{m-1})$, which is satisfied at the frequency minima, dephasing due to $\hat{S}_z$ is completely removed.

For superpositions of type $a|\pm,m\rangle + b|\pm,m-1\rangle$, the dephasing rate is given by

$$\frac{1}{T_2} = \frac{\alpha^2}{8}[\cos(\theta_m) - \cos(\theta_{m-1})]^2. \quad (50)$$

Here, there are two regions where the $\hat{S}_z$-caused dephasing is removed; when $\cos(\theta_m) = \cos(\theta_{m-1})$, which occurs at the frequency maxima, and at the high-field limit, where $\cos(\theta_m) = \cos(\theta_{m-1}) = 1 \; \forall \; m$, rendering such transitions as only NMR allowed

For superpositions of type $a|\pm, \pm(I + \frac{1}{2})\rangle + b|\pm,m\rangle$, the dephasing rate is given by

$$\frac{1}{T_2} = \frac{\alpha^2}{2}\sin\left(\frac{\theta_m}{2}\right)^4, \quad (51)$$

which reaches its minimal value of 0 as $B \to \infty$, whereas for superpositions of type $a|\pm, \pm(I + \frac{1}{2})\rangle + b|\mp,m\rangle$ it is given by

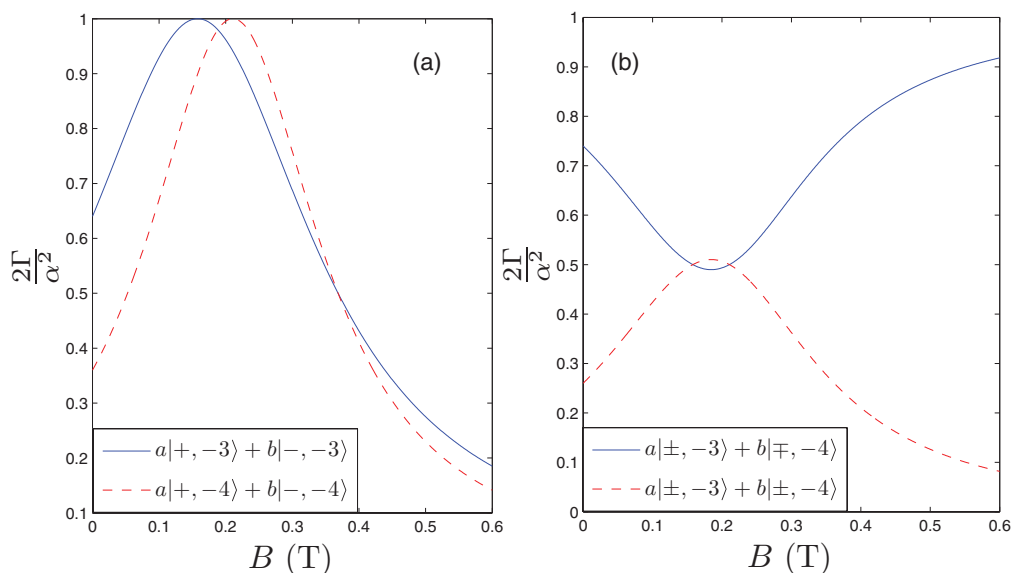$$\frac{1}{T_2} = \frac{\alpha^2}{2}\cos\left(\frac{\theta_m}{2}\right)^4, \quad (52)$$

FIG. 7. (Color online) The exponential decay rate given by Γ in units of $\alpha^2/2$ for diabatic Z noise driven (a) depolarization and (b) dephasing in Si:Bi. This is done in the four-dimensional subspace of $m = -3, m - 1 = -4$. (a) shows that in each subspace, the depolarization rate maximizes when $\theta_m = \pi/2$, or at the avoided crossing cancellation resonances. (b) shows that at the high-field limit, the dephasing rate of $a|\pm,m\rangle + b|\mp,m-1\rangle$ is maximal, whilst that of $a|\pm,m\rangle + b|\pm,m-1\rangle$ becomes vanishingly small. It should be noted, however, that the $a|-,m\rangle + b|+,m-1\rangle$ superposition cannot be made by either EPR or NMR in the high-field limit. These rates both approximately reach the value of 1/2 at the frequency minima.

which reaches its minimal value (that is generally greater than 0) at $B = 0$ T. The steady-state solution for adiabatic Z noise is given by

$$\underline{\mathbf{n}}(\infty) = \mathbb{1} \otimes \mathbb{1} + c_1 \mathbb{1} \otimes \hat{\sigma}_z + c_2 \hat{\sigma}_z \otimes \mathbb{1} + c_3 \hat{\sigma}_z \otimes \hat{\sigma}_z. \quad (53)$$

2. Diabatic Z noise

Here, we may set $\chi \to 0 \Rightarrow e^{-\chi \Omega^2} = 1 \; \forall \; \Omega^2$. Solving the Bloch vector differential equations yields analytic expressions for the dephasing rates. For an initial superposition of $a|\pm,m\rangle + b|\mp,m-1\rangle$, this gives

$$\frac{1}{T_2} = \frac{\alpha^2}{4}[\cos(\theta_m)\cos(\theta_{m-1}) + 1] \quad (54)$$

and for $a|\pm,m\rangle + b|\pm,m-1\rangle$,

$$\frac{1}{T_2} = \frac{\alpha^2}{4}[\cos(\theta_m)\cos(\theta_{m-1}) - 1]. \quad (55)$$

Equation (54) reaches a minimum value (hence giving the longest T_2 time) when $\cos(\theta_m) = -\cos(\theta_{m-1})$, i.e., at the frequency minima. Unlike the adiabatic Z noise case, this value does not reach 0, but rather reaches approximately half its maximal value at the high-field regime. Conversely, Eq. (55) reaches its maximal value when $\cos(\theta_m) = -\cos(\theta_{m-1})$, attaining approximately the same value as for Eq. (54) at this regime. Note that unlike the adiabatic case, there is no decoherence minimum at the frequency maxima; the decay rate simply vanishes as $B \to \infty$.

Because the exchange terms in Eq. (43) contribute to the dynamics for diabatic Z noise, there will also be depolarizing noise in each m subspace, equalizing the population in states $|\pm,m\rangle$. Figure 6(d) shows the effect of this depolarization at the frequency minima. The depolarization rate of each m subspace is given by

$$\frac{1}{T_1} = \frac{\alpha^2}{2}\sin(\theta_m)^2, \quad (56)$$

which vanishes as $B \to \infty$ and maximizes at the avoided crossing cancellation resonance. Given any superposition $\sqrt{P_g}|g\rangle + e^{i\phi}\sqrt{P_e}|e\rangle$, with states $|g\rangle$ and $|e\rangle$ each existing in a different m subspace, such that $\text{tr}[\hat{H}_0(|e\rangle\langle e| - |g\rangle\langle g|)] > 0$, the depolarization is given by

$$\text{tr}[\sigma_z \tilde{\rho}(t)] = \frac{1}{2}P_e\left(1 + e^{-t/T_1^e}\right) - \frac{1}{2}P_g\left(1 + e^{-t/T_1^g}\right), \quad (57)$$

where $1/T_1^{g/e}$ is the depolarization rate in the m subspace for $|g\rangle$ and $|e\rangle$, respectively. The steady-state solution for diabatic Z noise given such superpositions is given by

$$\underline{\mathbf{n}}(\infty) = \mathbb{1} \otimes \mathbb{1} + c_1 \hat{\sigma}_{\mathbf{z}} \otimes \mathbb{1}, \quad (58)$$

where $c_1 \in [1,-1]$. For superpositions of type $a|\pm, \pm(I + \frac{1}{2})\rangle + b|\pm,m\rangle$, the dephasing rate is given by

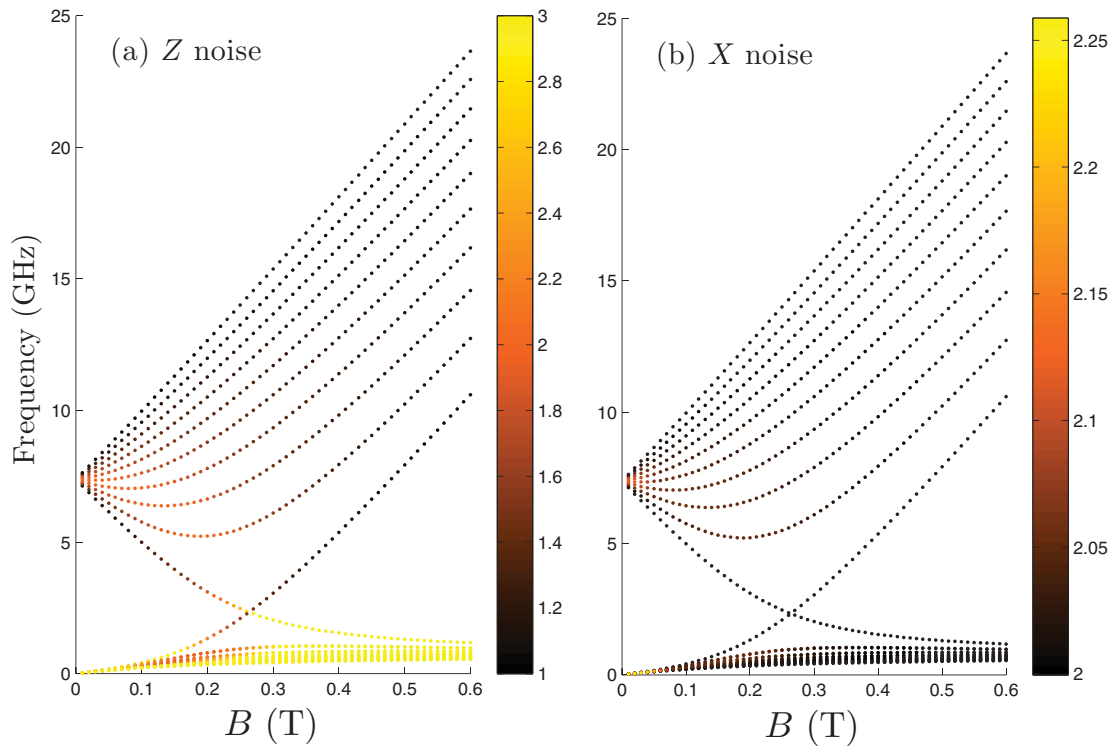$$\frac{1}{T_2} = \frac{\alpha^2}{4}[1 - \cos(\theta_m)] \quad (59)$$

FIG. 8. (Color online) Simulated dephasing times in units of $2/\alpha^2$ for diabatic (a) Z and (b) X noises, calculated with $\alpha^2/2\pi = 9$ MHz. In (a), the superpositions $a|\pm,m\rangle + b|\mp,m-1\rangle$ have T_2 times of $2/\alpha^2$ at $B \gtrsim 0.6$ T and approximately $4/\alpha^2$ at the frequency minima. Superpositions $a|\pm,m\rangle + b|\pm,m-1\rangle$ also have T_2 times of $4/\alpha^2$ at the frequency minima. However, as B increases, these become NMR transitions and will have T_2 times of $2/(\alpha^2 \delta)$. The color bar has been truncated after three to aid visibility but the maximum value reaches as high as ~ 100. In (b), the T_2 time does not vary by much and reaches its maximal points at fields less than the frequency minima.
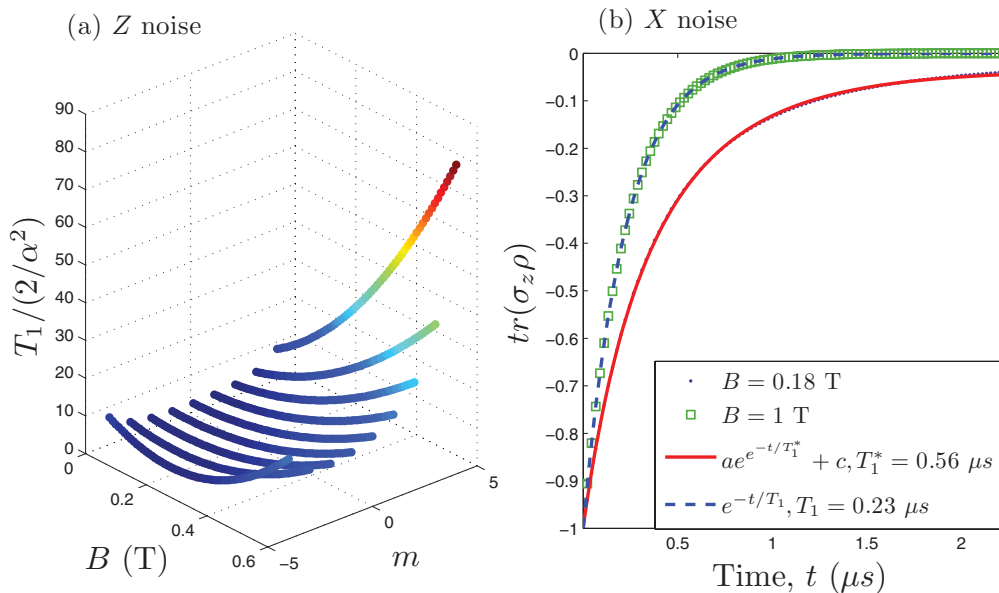
FIG. 9. (Color online) Simulated depolarizing times for diabatic Z and X noise with $\alpha^2/2\pi = 9$ MHz. (a) Given Z noise, the decay of $\mathrm{tr}[\sigma_z \tilde{\rho}(t)]$ within each m subspace is always exponential. For $m \leqslant 0$, the T_1 time reaches a minimum at the avoided crossing cancellation resonances. The T_1 times for subspaces m and $m - 1$ become identical at the frequency minima. (b) Given X noise, the decay in the $\{|+,m\rangle, |-,m-1\rangle\}$ and $\{|-,m\rangle, |+,m-1\rangle\}$ subspaces follows an exponential curve at high magnetic fields, but at low magnetic fields such as the frequency minima, it follows a double exponential fit.

and for superpositions of type $a|\pm, \pm(I + \frac{1}{2})\rangle + b|\mp,m\rangle$, the dephasing rate is given by

$$\frac{1}{T_2} = \frac{\alpha^2}{4}[1 + \cos(\theta_m)]. \tag{60}$$

The depolarization rate can be calculated as in the previous case, using Eq. (57) and noting that one of $T_1^{g/e}$ is equal to ∞. The steady-state solution for diabatic Z noise for such superpositions is given by

$$\underline{\mathbf{n}}(\infty) = \mathbb{1} \otimes \mathbb{1} + c_1 \hat{\sigma}_{\mathbf{z}} \otimes \mathbb{1} + c_2 \mathbb{1} \otimes \hat{\sigma}_{\mathbf{z}}. \tag{61}$$

For diabatic Z noise, Fig. 7 shows the analytical depolarization and dephasing rates for subspace $m = -3, m - 1 = -4$ in Si:Bi. Figure 8(a) shows the numerically calculated T_2 times for all EPR lines depicted in Fig. 2(b), whilst Fig. 9(a) shows the numerically calculated depolarising times T_1 in units of $2/\alpha^2$ for each m subspace.

B. X noise

X noise is less trivial, as it couples all components of the Hilbert space so we cannot consider a sub-Hamiltonian in isolation. Solving the resulting 400 Bloch equations (for Si:Bi) would be unfeasible, so only numerical calculations are given here. Furthermore, the adiabatic condition must be violated for X noise to have any effect, as there are no $\hat{S}_x(\Omega = 0)$ terms in Eq. (36). In the high-field limit, the X noise operator will take the form of $\hat{\sigma}_x \otimes \mathbb{1}$ in the basis $\{|+,m\rangle, |-,m-1\rangle\}$ as well as $\{|-,m\rangle, |+,m-1\rangle\}$. At such fields, as shown in Fig. 6(c), an arbitrary superposition of $a|\pm,m\rangle + b|\mp,m-1\rangle$ suffers a two-level system depolarizing channel. At low fields, however, the dissipation is not contained within the $m, m - 1$ subspace,

and as indicated by Fig. 6(b) the system eventually decays to $\frac{1}{d}\mathbb{1}$.

For X noise, all dephasing is a result of the depolarising noise that is affected by the X noise operator, and as shown in Fig. 8(b), at $B > 0.6$ T, the dephasing time is $4/\alpha^2$ for all transitions. This value increases only slightly at magnetic fields smaller than the frequency minima for transitions involving $m < 0$.

Figure 9(b) shows the different forms of depolarising rates for X noise. At high magnetic fields, where the only nonvanishing matrix elements of the X noise operator are $\langle \pm,m|\hat{S}_x|\mp,m-1\rangle$, the depolarizing noise follows an exponential decay. Under intermediate magnetic fields, however, the dissipation follows a more complicated mechanism and the decay is better explained by a double exponential fit.

V. CONCLUSIONS

A coupled nuclear-electronic spin system with large hyperfine coupling strength A will have its eigenstates as superpositions of the z-axis spin basis states at appreciably large magnetic fields, which we call the intermediate-field regime. This will allow for performing EPR transitions between eigenstates that, at high-field, are EPR forbidden and would require NMR pulses, which are orders of magnitude slower. We have shown that this allows for two-qubit universal quantum computation to be performed with only the use of EPR pulses. Si:P has $A/2\pi = 117.5$ MHz, so it will be in the intermediate-field regime when $B \sim 0.02$ T. At such a low field, the transition frequencies are of the order $\lesssim 0.5$ GHz. With Si:Bi, on the other hand, with $A/2\pi = 1.4754$ GHz, the intermediate-field condition is satisfied when $B \sim 0.5$ T and the transition frequencies are of order $\lesssim 10$ GHz. For current

EPR technology, operation in the intermediate-field regime is easier to carry out on Si:Bi. Indeed, this has been recently demonstrated experimentally in Ref. 12.

For a nuclear-electronic spin system with $I \geqslant 1$, cancellation resonances can be seen at nonvanishing magnetic fields; Si:P has only one cancellation resonance at $B \simeq 0$ T, whereas Si:Bi has a series of cancellation resonances at $B \lesssim 0.3$ T. Furthermore, interesting effects such as decoherence reduction, associated with $df/dB = 0$ points, occur between eigenstates belonging to two different subspaces that have a cancellation resonance. As a result, Si:P with $I = 1/2$ does not have any $df/dB = 0$ regions and hence no decoherence reduction points, whereas Si:Bi with $I = 9/2$ has several. The combination of fast EPR quantum gates and decoherence reduction makes Si:Bi an attractive system for quantum information processing.

ACKNOWLEDGMENTS

APPENDIX A: SELECTIVE ROTATIONS

Consider the coupled nuclear-electronic spin system in the eigenbasis of the Hamiltonian $\hat{H}_0$ given by Eq. (1). The electron spin operators in this basis are given by the unitary transformation

$$\hat{S}'_x = V^\dagger \hat{S}_x V \quad \text{and} \quad \hat{S}'_y = V^\dagger \hat{S}_y V, \tag{A1}$$

where V is a matrix whose ith column is the ith eigenvector of $\hat{H}_0$. We want to be able to isolate two eigenstates of this Hamiltonian, and perform unitary dynamics in that subspace. Tracing out all eigenvectors other than $|e\rangle$ and $|g\rangle$ gives

$$(\hat{S}'_x)^{eg} = \frac{1}{2}\begin{pmatrix} 0 & |e\rangle\langle e|(\hat{S}_+ + \hat{S}_-)|g\rangle\langle g| \\ |g\rangle\langle g|(\hat{S}_+ + \hat{S}_-)|e\rangle\langle e| & 0 \end{pmatrix}$$
$$= \frac{\eta}{2}\hat{\sigma}_x,$$

$$(\hat{S}'_y)^{eg} = \frac{i}{2}\begin{pmatrix} 0 & |e\rangle\langle e|(\hat{S}_- - \hat{S}_+)|g\rangle\langle g| \\ |g\rangle\langle g|(\hat{S}_- - \hat{S}_+)|e\rangle\langle e| & 0 \end{pmatrix}$$
$$= \text{sign}_y \frac{\eta}{2}\hat{\sigma}_y, \tag{A2}$$

where $\eta = \langle e|\hat{S}_x|g\rangle$ is a measure of basis state mixing and $\text{sign}_y = \langle e|\hat{S}_z + \hat{I}_z|e\rangle - \langle g|\hat{S}_z + \hat{I}_z|g\rangle \in \{1, -1\}$. As the absolute energies given by the eigenvalues are meaningless physically, we can rescale the eigenvalues of $\hat{H}_0$ by adding to it an identity term $-\frac{(\lambda_e + \lambda_g)}{2}\mathbb{1}$ such that λ_e and λ_g are the eigenvalues of eigenvectors $|e\rangle$ and $|g\rangle$, respectively, where $\lambda_e > \lambda_g$. This gives

$$\hat{H}_0 \mapsto \hat{H}_0^\varsigma = \frac{\Omega_0}{2}\hat{\sigma}_z^{eg} \oplus \hat{H}_0^{\text{rem}}, \tag{A3}$$

such that $\Omega_0 = |\lambda_e - \lambda_g|$, and σ_z^{eg} is exists in the $\{|e\rangle, |g\rangle\}$ subspace. Given a perturbative Hamiltonian of the form in Eq. (26), and assuming that all EPR-allowed transition frequencies are unique, we may solve the Liouville-von Neumann equation for the two-level subsystem in the rotating frame of $\hat{H}_0^\varsigma$, while making the rotating wave approximation:

$$\frac{d}{dt}\tilde{\rho}(t) = i\frac{\omega_1}{2}[\tilde{\rho}(t), e^{itH_0^\varsigma}\{[\cos(\Omega_0 t)(\hat{S}'_{x/y})^{eg}$$
$$+ \sin(\Omega_0 t)(\hat{S}'_{y/x})^{eg}] + [\cos(\Omega_0 t)(\hat{S}'_{x/y})^{eg}$$
$$- \sin(\Omega_0 t)(\hat{S}'_{y/x})^{eg}]\}e^{-itH_0^\varsigma}]$$
$$= i\frac{\omega_1\eta}{4}[\tilde{\rho}(t), \hat{\sigma}_{x/y}] + i\frac{\omega_1\eta}{4}[\tilde{\rho}(t), \cos(2\Omega_0 t)\hat{\sigma}_{x/y}$$
$$- \sin(2\Omega_0 t)\hat{\sigma}_{y/x}]$$
$$\approx i\frac{\omega_1\eta}{4}[\tilde{\rho}(t), \hat{\sigma}_{x/y}] \text{ if } \omega_1 \ll \Omega_0. \tag{A4}$$

There are two possible regimes for the dynamics of this system. Those for which sign_y is positive (negative), which occurs when increasing the energy of the system corresponds to an increase (decrease) in z-axis total magnetisation m. In the case that $\text{sign}_y = 1$, the circular polarization needed to achieve resonance with the Hamiltonian is of the form $\cos(\Omega_0 t)\hat{S}_{x/y} + \sin(\Omega_0 t)\hat{S}_{y/x}$. We call this the right-handed (RH) field. When $\text{sign}_y = -1$, the circular polarization must be of the form $\cos(\Omega_0 t)\hat{S}_{x/y} - \sin(\Omega_0 t)\hat{S}_{y/x}$, which we call the left-handed (LH) field. Table IV shows the form that matrices $(\hat{S}'_{x/y})^{eg}$ take for both regimes and the polarization of the magnetic field required to achieve resonance.

TABLE IV. Pauli operators for the truncated two-level system under resonance in the right-handed and left-handed regimes. The bottom row indicates the polarization that the $V_{x/y}(t)$ term must have in order to effect a $e^{\pm i\frac{\theta}{2}\hat{\sigma}_{x/y}}$ operator in the rotating frame.

	Right-handed	Left-handed
sign_y	$\langle e|\hat{S}_z + \hat{I}_z|e\rangle - \langle g|\hat{S}_z + \hat{I}_z|g\rangle = 1$	$\langle e|\hat{S}_z + \hat{I}_z|e\rangle - \langle g|\hat{S}_z + \hat{I}_z|g\rangle = -1$
$(\hat{S}'_x)^{eg}$	$\frac{1}{2}\begin{pmatrix} 0 & |e\rangle\langle e|\hat{S}_+|g\rangle\langle g| \\ |g\rangle\langle g|\hat{S}_-|e\rangle\langle e| & 0 \end{pmatrix} = \frac{\eta}{2}\hat{\sigma}_x$	$\frac{1}{2}\begin{pmatrix} 0 & |e\rangle\langle e|\hat{S}_-|g\rangle\langle g| \\ |g\rangle\langle g|\hat{S}_+|e\rangle\langle e| & 0 \end{pmatrix} = \frac{\eta}{2}\hat{\sigma}_x$
$(\hat{S}'_y)^{eg}$	$\frac{i}{2}\begin{pmatrix} 0 & -|e\rangle\langle e|\hat{S}_+|g\rangle\langle g| \\ |g\rangle\langle g|\hat{S}_-|e\rangle\langle e| & 0 \end{pmatrix} = \frac{\eta}{2}\hat{\sigma}_y$	$\frac{i}{2}\begin{pmatrix} 0 & |e\rangle\langle e|\hat{S}_-|g\rangle\langle g| \\ -|g\rangle\langle g|\hat{S}_+|e\rangle\langle e| & 0 \end{pmatrix} = -\frac{\eta}{2}\hat{\sigma}_y$
$(\hat{H}_o^\varsigma)^{eg}$	$\frac{\Omega_0}{2}\hat{\sigma}_z$	$\frac{\Omega_0}{2}\hat{\sigma}_z$
rotating field	$\cos(\Omega_0 t)\hat{S}_{x/y} + \sin(\Omega_0 t)\hat{S}_{y/x}$	$\cos(\Omega_0 t)\hat{S}_{x/y} - \sin(\Omega_0 t)\hat{S}_{y/x}$

APPENDIX B: MASTER EQUATION DERIVATION

Taking the Hamiltonian from Eq. (1) and adding to it a perturbative term involving independent temporal magnetic-field fluctuations in all three spatial dimensions, all of which take a Gaussian distribution with mean 0 and variance α_n^2, gives in the interaction picture:

$$\tilde{H}(t) = \sum_{n=1}^{3} \omega_n(t)\tilde{S}_n(t) + \omega_n(t)\delta \tilde{I}_n(t), \qquad \text{(B1)}$$

where $\{S_n\}$ and $\{I_n\}$ are the n-axis electron and nuclear spin operators, respectively, and $\omega_n(t)$ is the corresponding electron Zeeman frequency at time t. As before, δ represents the ratio of the nuclear to electronic Zeeman frequencies, and as it is small, we may ignore the nuclear term. We then write the Liouville-von Neumann equation in differential-integral form and take the average over the field fluctuations. Noting that $\langle \frac{d}{dt}\tilde{\rho}(t)\rangle = \frac{d}{dt}\langle\tilde{\rho}(t)\rangle$ we may write this as

$$\frac{d}{dt}\langle\tilde{\rho}(t)\rangle = i\sum_{n=1}^{3}\langle\omega_n(t)\rangle[\langle\tilde{\rho}(t)\rangle,\tilde{S}_n(t)] - \sum_{n=1}^{3}\int_{t_0}^{t}ds$$
$$\times \langle\omega_n(t)\omega_n(s)\rangle[[\langle\tilde{\rho}(t)\rangle,\tilde{S}_n^\dagger(t)],\tilde{S}_n(s)], \quad \text{(B2)}$$

where assigning $\tilde{S}_n(t) = \tilde{S}_n^\dagger(t)$ is valid as it is a Hermitian operator. $\langle\tilde{\rho}(t)\rangle$ is the density operator for the nuclear-electronic system, averaged either over an ensemble of such systems, or over many repeated experiments on the same system. Here, we have assumed that the field fluctuation statistics are independent of the quantum state of our system. These assumptions and approximations lead to a Born-Markov master equation. As $\omega_n(t)$ follows a Gaussian distribution with mean 0, the first term of this equation vanishes. Given that the correlation function drops to zero at finite values, we may set the integration limits to $t_0 = 0$ and $t = \infty$, and change the integration constant to $\tau = t - s$. As the temporal fluctuation takes a Gaussian distribution, we may set our correlation functions to be another Gaussian function of the form

$$\langle\omega_n(t)\omega_n(t-\tau)\rangle = \frac{\alpha_n^2}{2\sqrt{\pi}\chi_n}e^{-\frac{\tau^2}{4\chi_n}}, \qquad \text{(B3)}$$

where $\chi_n = (dB_n/dt)^{-1}$ is an inverse function of how fast the magnetic field fluctuates. In the limiting case of $dB_n/dt \to \infty$, the correlation function tends to $\alpha_n^2\delta(\tau)$. To aid our calculation, we may write the noise operators in the basis of the eigenstates of $\hat{H}_0$ labeled $\{|a\rangle,|b\rangle\}$:

$$\hat{S}_n = \sum_\Omega \hat{S}_n(\Omega),$$
$$\hat{S}_n(\Omega) = \sum_{a,b}\delta(\omega_{ba} - \Omega)|a\rangle\langle a|\hat{S}_n|b\rangle\langle b|. \qquad \text{(B4)}$$

Moving such operators to the interaction picture simply gives $e^{-i\Omega t}\hat{S}_n(\Omega)$. This gives

$$\frac{d}{dt}\langle\tilde{\rho}(t)\rangle = -\alpha_n^2\sum_{n=1}^{3}\sum_{\Omega,\Omega'}\int_0^\infty\frac{d\tau}{2\sqrt{\pi}\chi_n}e^{-\frac{\tau^2}{4\chi_n}}e^{i\Omega\tau}e^{it(\Omega'-\Omega)}$$
$$\times[[\langle\tilde{\rho}(t)\rangle,\hat{S}_n^\dagger(\Omega')],\hat{S}_n(\Omega)]. \qquad \text{(B5)}$$

If $\alpha^2 \ll \Omega,\Omega'$, meaning that the dynamic time scale of our system is much shorter than that of the decoherence caused by the magnetic-field fluctuation, which is a reasonable assumption for systems of interest, we may make the rotating wave approximation (often also referred to as the secular approximation) and drop all terms where $\Omega \neq \Omega'$. Furthermore, noting that $[A,[B,C]] = ABC - BCA + \text{H.c.}$ (Hermitian conjugate) if A,B,C are Hermitian operators leads to

$$\frac{d}{dt}\langle\tilde{\rho}(t)\rangle = \alpha_n^2\sum_{n=1}^{3}\sum_\Omega\int_0^\infty\frac{d\tau}{2\sqrt{\pi}\chi_n}e^{-\frac{\tau^2}{4\chi_n}}e^{i\Omega\tau}$$
$$\times[\hat{S}_n^\dagger(\Omega)\langle\tilde{\rho}(t)\rangle\hat{S}_n(\Omega) - \langle\tilde{\rho}(t)\rangle\hat{S}_n^\dagger(\Omega)\hat{S}_n(\Omega)]$$
$$+ \text{H.c.}$$
$$\text{(B6)}$$

We may decompose the integrand to

$$\int_0^\infty\frac{d\tau}{2\sqrt{\pi}\chi_n}e^{-\frac{\tau^2}{4\chi_n}}e^{i\Omega\tau} = \upsilon_n(\Omega) + i\Upsilon_n(\Omega), \qquad \text{(B7)}$$

where

$$\upsilon_n(\Omega) = \frac{1}{2}\int_{-\infty}^{\infty}\frac{d\tau}{2\sqrt{\pi}\chi_n}e^{-\frac{\tau^2}{4\chi_n}}e^{i\Omega\tau} = \frac{1}{2}e^{-\chi_n\Omega^2},$$
$$\Upsilon_n(\Omega) = \frac{1}{2i}\int_0^\infty\frac{d\tau}{2\sqrt{\pi}\chi_n}e^{-\frac{\tau^2}{4\chi_n}}(e^{i\Omega\tau} - e^{-i\Omega\tau}).$$
$$\text{(B8)}$$

Plugging these expressions into Eq. (B6) and moving back into the Schrödinger picture, gives us our final master equation:

$$\frac{d}{dt}\langle\rho(t)\rangle = i[\langle\rho(t)\rangle,\hat{H}_0 + \hat{H}_{LS}]$$
$$+ \alpha_n^2\sum_{n=1}^{3}\sum_\Omega e^{-\chi_n\Omega^2}\left\{\hat{S}_n^\dagger(\Omega)\langle\tilde{\rho}(t)\rangle\hat{S}_n(\Omega)\right.$$
$$\left.- \frac{1}{2}[\langle\tilde{\rho}(t)\rangle,\hat{S}_n^\dagger(\Omega)\hat{S}_n(\Omega)]_+\right\}, \qquad \text{(B9)}$$

where

$$H_{LS} = \sum_n\sum_\Omega\Upsilon_n(\Omega)\hat{S}_n^\dagger(\Omega)\hat{S}_n(\Omega) \qquad \text{(B10)}$$

is the Lamb shift and changes the energy levels of the system. This is a negligible effect and hence can be ignored. We use $[A,B]_+ := AB + BA$ as the anticomutator operator.

---

*m.mohammady@ucl.ac.uk

†Present address: Department of Physics, University of Warwick, Gibbet Hill Road, Coventry CV4 7AL, UK.

[1]B. E. Kane, Nature (London) **393**, 133 (1998).

[2]S. R. Schofield, N. J. Curson, M. Y. Simmons, F. J. Rueß, T. Hallam, L. Oberbeck, and R. G. Clark, Phys. Rev. Lett. **91**, 136104 (2003); A. M. Tyryshkin, S. A. Lyon, A. V. Astashkin, and A. M. Raitsimring, Phys. Rev. B **68**, 193207 (2003); Kai-Mei C. Fu,

T. D. Ladd, C. Santori, and Y. Yamamoto, *ibid.* **69**, 125306 (2004); G. W. Morley, D. R. McCamey, H. A. Seipel, L.-C. Brunel, J. van Tol, and C. Boehme, Phys. Rev. Lett **101**, 207602 (2008); J. J. L. Morton, A. M. Tyryshkin, R. M. Brown, S. Shankar, B. W. Lovett, A. Ardavan, T. Schenkel, E. E. Haller, J. W. Ager, and S. A. Lyon, Nature (London) **455**, 1085 (2008); A. Morello *et al.*, *ibid.* **467**, 687 (2010); D. R. McCamey, C. Boehme, G. W. Morley, and J. van Tol, Phys. Rev. B **85**, 073201 (2012); P. T. Greenland, S. A. Lynch, A. F. G. van der Meer, B. N. Murdin, C. R. Pidgeon, B. Redlich, N. Q. Vinh, and G. Aeppli, Nature (London) **465**, 1057 (2010); M. Steger, T. Sekiguchi, A. Yang, K. Saeedi, M. E. Hayden, M. L. W. Thewalt, K. M. Itoh, H. Riemann, N. V. Abrosimov, P. Becker, and H. J. Pohl, J. Appl. Phys. **109**, 102411 (2011); S. Simmons, R. M. Brown, H. Riemann, N. V. Abrosimov, P. Becker, H. J. Pohl, M. L. W. Thewalt, K. M. Itoh, and J. J. L. Morton, Nature (London) **470**, 69 (2011).

[3]H. Morishita, L. S. Vlasenko, H. Tanaka, K. Semba, K. Sawano, Y. Shiraki, M. Eto, and K. M. Itoh, Phys. Rev. B **80**, 205206 (2009).

[4]G. W. Morley, M. Warner, A. M. Stoneham, P. T. Greenland, J. van Tol, C. W. M. Kay, and G. Aeppli, Nat. Mater. **9**, 725 (2010).

[5]R. E. George, W. Witzel, H. Riemann, N. V. Abrosimov, N. Nötzel, M. L. W. Thewalt, and J. J. L. Morton, Phys. Rev. Lett. **105**, 067601 (2010).

[6]T. Sekiguchi, M. Steger, K. Saeedi, M. L. W. Thewalt, H. Riemann, N. V. Abrosimov, and N. Nötzel, Phys. Rev. Lett. **104**, 137402 (2010).

[7]M. H. Mohammady, G. W. Morley, and T. S. Monteiro, Phys. Rev. Lett. **105**, 067602 (2010).

[8]M. Belli, M. Fanciulli, and N. V. Abrosimov, Phys. Rev. B **83**, 235204 (2011).

[9]W. M. Witzel and S. Das Sarma, Phys. Rev. B **74**, 035322 (2006).

[10]Wen Yang and Ren-Bao Liu, Phys. Rev. B **78**, 085315 (2008).

[11]Alexei M. Tyryshkin, S. Tojo, J. J. L. Morton, H. Riemann, N. V. Abrosimov, P. Becker, H.-J. Pohl, T. Schenkel, M. L. W. Thewalt, K. M. Itoh, and S. A. Lyon, e-print arXiv:1105.3772v1 (unpublished).

[12]G. W. Morley, P. Lueders, M. H. Mohammady, S. J. Balian, G. Aeppli, C. W. M. Kay, W. M. Witzel, G. Jeschke, and T. S. Monteiro, e-print arXiv:1109.4269 (unpublished).

[13]A. Schweiger and G. Jeschke, *Principles of Pulse Paramagnetic Resonance* (Oxford University Press, Great Clarendon Street, Oxford, UK, 2001).

[14]G. Ithier, E. Collin, P. Joyez, P. J. Meeson, D. Vion, D. Esteve, F. Chiarello, A. Shnirman, Y. Makhlin, J. Schriefl, and G. Schon, Phys. Rev. B **72**, 134519 (2005); D. Vion, A. Aassime, A. Cottet, P. Joyez, H. Pothier, C. Urbina, D. Esteve, and M. H. Devoret, Science **296**, 886 (2002).

[15]G. Mitrikas, Y. Sanakis, and G. Papavassiliou, Phys. Rev. A **81**, 020305(R) (2010).

[16]D. P. DiVincenzo, Phys. Rev. A **51**, 1015 (1995).

[17]Michael A. Nielsen and Issac L. Chuang, *Quantum Computation and Quantum Information* (Cambridge university press, The Edinburgh Building, Cambridge, UK, 2000).

[18]A. M. Stoneham, A. J. Fisher, and P. T. Greenland, J. Phys. Condens. Matter **15**, L447 (2003); A. M. Stoneham, A. H. Harker, and G. W. Morley, J. Phys. Condens. Matter **21**, 364222 (2009).

[19]G. Burkard, D. Loss, D. P. Di Vincenzo, and J. A. Smolin, Phys. Rev. B **60**, 11404 (1999).

[20]P. W. Anderson, *Concepts in Solids* (Addison Wesley, Redwood City, 1963).

[21]N. Schuch and J. Siewert, Phys. Rev. A **67**, 032301 (2003).

[22]Y. Makhlin, Quant. Info. Proc. **1**, 243 (2002).

[23]H. P. Breuer and F. Petruccione, *The Theory of Open Quantum Systems* (Oxford University Press, Great Clarendon Street, Oxford, UK, 2007).

[24]D. M. Tong, K. Singh, L. C. Kwek, and C. H. Oh, Phys. Rev. Lett. **95**, 110407 (2005).

[25]G. Feher and E. A. Gere, Phys. Rev. **114**, 1245 (1959).

[26]T. G. Castner, Phys. Rev. **155**, 816 (1967).

[27]D. P. S. McCutcheon, A. Nazir, S. Bose, and A. J. Fisher, Phys. Rev. A **80**, 022337 (2009).